

Multivariate Temporal Point Process Regression

Xiwei Tang and Lexin Li

Abstract

Point process modeling is gaining increasing attention, as point process data are widely emerging in various scientific applications. Motivated by a neuronal spike trains study, we propose a novel point process regression model for multivariate response and predictor processes in this article. Our key idea is to incorporate the predictor effects into the conditional intensity functions using a set of basis transferring functions in a convolutional fashion. We further impose low-rank, sparsity and subgrouping structures on the transferring coefficients that are organized in the form of a three-way tensor. We develop a highly scalable optimization algorithm for parameter estimation, and establish the large sample error bound for the recovered transferring coefficient tensor and the subgroup identification consistency. Unlike most existing point process modeling approaches, our proposal allows the dimensions of both the response and predictor processes to diverge, and does not require the stationary condition. It permits a general class of link functions and multiple basis functions. Moreover, multiple point processes are modeled in a joint fashion, rather than one at a time. The estimator is shown asymptotically to benefit not only from increasing length of observation time, but also from increasing dimensions of the response and predictor processes. We illustrate the empirical performance of our method through simulations and a cross-area neuronal spike trains analysis in a sensory cortex study.

Key Words: Hawkes process; Neuronal spike trains; Point process; Regularization; Tensor decomposition.

¹Xiwei Tang is Assistant Professor, Department of Statistics, University of Virginia. Email: xt4yj@virginia.edu. Lexin Li is Professor, and the corresponding author, Department of Biostatistics and Epidemiology, University of California, Berkeley. Email: lexinli@berkeley.edu

1 Introduction

Point process is drawing increasing attention in recent years, as data taking the form of point process are rapidly emerging in a wide variety of applications. Examples include forest ecology (Stoyan et al., 2000; Guan et al., 2015), spatial epidemiology (Diggle et al., 2010), social network modeling (Perry and Wolfe, 2013), neuronal activity modeling (Brown et al., 2004; Cunningham et al., 2008; Pillow et al., 2008), functional neuroimaging meta analysis (Kang et al., 2011, 2014), among others. In general, a point process is a collection of events, or points, randomly located in some domain space, e.g., a spatial domain or a time domain. Our motivation is a neuronal spike trains analysis in a sensory cortex study (Okun et al., 2015). A newly developed two-photon calcium imaging technique is now greatly facilitating neuroscience studies, as it enables scientists to simultaneously record the dynamic activities for a population of neurons while maintaining individual neuron resolution (Ji et al., 2016). In our study, there are 139 and 283 neurons imaged simultaneously from two areas of a rat’s brain, the primary visual cortex area (V1) and the primary auditory cortex area (A1). In a visual activity, it is known that, some locations of the primary visual cortex would respond to input from auditory and other sensory areas (Liang et al., 2013). One of the scientific goals of this study is to understand the association patterns and information transmissions between individual neurons across A1 and V1, and to model potential excitation or inhibitory effects of neuron firings between the two areas.

In this article, we propose a novel multivariate point process regression model to address this question. Our new model allows both responses and predictors to be high-dimensional point processes. Our key idea is to incorporate the predictor effects into the conditional intensity functions using a set of basis transferring functions in a convolutional fashion. To further reduce the dimension of the parameter space, we impose a low-rank structure on the transferring coefficients that are organized in the form of a three-way tensor. Consequently, the coefficient tensor that captures the association patterns between the response and predictor processes is characterized by a relatively small number of latent factors. We further introduce a set of penalty functions to accommodate additional structures of sparsity and subgrouping to facilitate both model interpretation and parameter reduction. Both low-rank and sparsity are commonly used low-dimensional structures in high-dimensional regression analysis (Chen et al., 2019a), and are scientifically plausible in neuroscience and many other applications (Zhou et al., 2013a; Sun and Li, 2017; Zhang and Han,

2019). Subgrouping is another common structure in plenty of applications, and it corresponds to ensemble neural activity in neuroscience (Okun et al., 2015). Together these structures enable us to jointly model and integrate information across individual point processes for both response and predictor processes. We then develop a highly scalable alternating direction method of multipliers (ADMM) for parameter estimation. Next we establish the asymptotic properties of the penalized maximum likelihood estimator while allowing the dimensions of both the response and predictor processes to diverge. We show that, the diverging dimensions actually benefit the estimation, yielding a faster convergence rate on the asymptotic concentration, which turns the adversity of the high-dimensionality of data into an advantage. Finally, we remark that, in our model, the predictors are not limited to any particular type of point process, but instead can handle different types of stochastic process as well as designed signals. Moreover, although motivated by a neuroscience problem, our method is equally applicable to many other point process applications, for example, the social infection network learning (Zhou et al., 2013b).

Our proposal differs considerably from the existing literature on point process modeling in multiple ways. First, the conventional inhomogeneous point process solutions mostly target a univariate or bivariate process (Diggle et al., 2010; Liang et al., 2008; Waagepetersen and Guan, 2009), along with a limited number of predictors. We instead aim to model high-dimensional multivariate point processes for both responses and predictors, and we allow the dimensions of both processes to diverge. Second, numerous point process methods focus on spatial point processes, where the events are located in a spatial domain (e.g., Guan, 2008; Guan et al., 2015; Kang et al., 2011, 2014). We however aim at evolutionary temporal point processes, where the events reside in a temporal domain. Such a difference implies different model assumptions and modeling techniques. For an inhomogeneous spatial point process, its intensity function is often assumed to depend on some location-relevant random variables (Diggle, 2013). For a temporal point process, however, it is usually assumed that the recurrent events are evolutionary in nature, in that the occurrence of a future event depends on the historical realizations of the process. Third, there have been a family of methods proposed to model evolutionary temporal point process, all of which are built on a self-exciting process called the Hawkes process that models the intensity function through the past event times (Hawkes, 1971). Such methods are also commonly used in neuronal spike trains analysis. Our proposal is closely related to but also clearly distinctive of this family of methods, in terms of model assumptions, modeling strategies, as well as theoretical properties. Specifically,

Zhou et al. (2013b); Bacry et al. (2015) imposed a linear intensity function and considered only a univariate basis function for transferring effect. Hansen et al. (2015) assumed a stationary point process and required the dimension of point process to be fixed. Bacry and Muzy (2016) again fixed the dimension of point process and employed a moment-based estimation method. Chen et al. (2019b) studied a Hawkes model without requiring non-negative transferring functions, but modeled each individual point process separately, in that the model parameters are estimated for one point process at a time. By contrast, we propose an utterly different solution that does not particularly rely on Hawkes process. As for model assumptions, we permit a general class of link functions that can be nonlinear, as well as multiple nonlinear basis functions, and do not require the stationary condition. Moreover, we allow the dimensions of the response and predictor processes to diverge. As for modeling strategies, we adopt an intensity-based instead of moment-based approach. More importantly, we model multiple point processes in a joint fashion, rather than one at a time. As for theoretical properties, our estimation method is to benefit not only from increasing length of observation time of the processes, as all existing approaches for multivariate Hawkes processes do, but also to benefit from increasing dimensions of the response and predictor processes. For those reasons, we believe our method makes a unique and useful addition to the toolbox of multivariate temporal point process modeling.

The rest of the article is organized as follows. Section 2 provides a brief review of temporal point process. Section 3 introduces our proposed multivariate temporal point process regression model. Section 4 develops the estimation algorithm, and Section 5 establishes the theoretical properties. Section 6 presents the simulations, and Section 7 illustrates with a neuronal spike trains data analysis. All technical proofs are relegated to the Supplementary Materials.

2 Background

2.1 Basic concepts

We begin with a brief review of temporal point process, and we refer to Daley and Vere-Jones (2007) for more details. Specifically, a temporal point process is a stochastic counting process defined on the positive half of the real line \mathbb{R}^+ , and taking non-negative integer values. For a univariate process $X(t)$, let $t_1, t_2, \dots \in \mathbb{R}^+$ denote the event times, under which $X(A) = \sum_{l=1} \mathbf{1}_{[t_l \in A]}$ for any $A \in \mathcal{B}(\mathbb{R}^+)$, and $\mathcal{B}(\mathbb{R}^+)$ denotes the Borel σ -algebra of \mathbb{R}^+ . Define its mean intensity func-

tion as $\Lambda(t) = \lim_{dt \rightarrow 0} \mathbb{E}[dX(t)]/dt$, where $dX(t) = X([t, t + dt))$, and dt is an arbitrary small increment of time. A temporal point process is homogeneous if its mean intensity is a constant, and is inhomogeneous otherwise. If $\Lambda(t)$ is also a stochastic process, then it is a doubly stochastic process; e.g., a Cox process. A temporal point process is usually assumed to be orderly; i.e., $\Pr(dX(t) > 1) = o(dt)$, which implies that $\Lambda(t) = \Pr(dX(t) = 1)$. In addition, a point process $X(t)$ is stationary, if the distribution of $dX(t)$ only depends on the length of dt but not the location t on the time line. It is straightforward to generalize the notion of a univariate point process to a multivariate point process, i.e., $\mathbf{X}(t) = (X_1(t), \dots, X_p(t))^T$.

2.2 Moment statistics and conditional intensity function

The first-order and second-order moment statistics of a point process are often of great interest, as they are usually sufficient to characterize the entire process. Consider a p -dimensional multivariate point process $\mathbf{X}(t)$, and assume it is stationary. Define its first-order moment statistic, i.e., the mean intensity, and its second-order statistic, i.e., the cross-covariance, as,

$$\Lambda_i^x = \mathbb{E}\{dX_i(t)\}/dt, \quad i = 1, \dots, p,$$

$$V_{ij}^x(\tau) = \mathbb{E}\{dX_i(t)dX_j(t - \tau)\}/\{dtd(t - \tau)\} - \Lambda_i\Lambda_j - \delta_{ij}(\tau)\Lambda_i, \quad i, j = 1, \dots, p,$$

respectively, where $\delta_{ij}(\tau) = 0$ if $i \neq j$, and $\delta_{ij}(\tau) = \delta(\tau)$ if $i = j$, and $\delta(\cdot)$ denotes the Dirac delta function satisfying that $\delta(x) = 0$ for $x \neq 0$ and $\int_{-\infty}^{+\infty} \delta(x)dx = 1$. Write $\mathbf{\Lambda}^x = (\Lambda_1^x, \dots, \Lambda_p^x)^T \in \mathbb{R}^p$, and $\mathbf{V}^{xx}(\cdot) = (V_{ij}^x(\cdot)) : \mathbb{R} \mapsto \mathbb{R}^{p \times p}$. Next, consider another stationary m -dimensional multivariate point process $\mathbf{Y}(t)$, and define its mean intensity $\mathbf{\Lambda}^y = (\Lambda_1^y, \dots, \Lambda_m^y)^T \in \mathbb{R}^m$, and cross-covariance $\mathbf{V}^{yy}(\cdot) = (V_{ij}^y(\cdot)) : \mathbb{R} \mapsto \mathbb{R}^{m \times m}$ accordingly. Define the cross-covariance between $X_j(t)$ and $Y_i(t)$ as,

$$C_{ji}^{xy}(\tau) = \mathbb{E}\{dX_j(t)dY_i(t - \tau)\}/\{dtd(t - \tau)\} - \Lambda_j^x\Lambda_i^y, \quad i = 1, \dots, m, j = 1, \dots, p.$$

Write $\mathbf{C}^{xy}(\cdot) = (C_{ji}^{xy}(\cdot)) : \mathbb{R} \mapsto \mathbb{R}^{p \times m}$, and $\mathbf{C}^{yx}(\cdot) = (C_{ij}^{yx}(\cdot)) : \mathbb{R} \mapsto \mathbb{R}^{m \times p}$. Note that, for any τ , it holds that $\mathbf{V}_{jj'}^{xx}(\tau) = \mathbf{V}_{j'j}^{xx}(-\tau)$, $j, j' = 1, \dots, p$, $\mathbf{V}_{i'i'}^{yy}(\tau) = \mathbf{V}_{i'i}^{yy}(-\tau)$, $i, i' = 1, \dots, m$, and $\mathbf{C}_{ji}^{xy}(\tau) = \mathbf{C}_{ij}^{yx}(-\tau)$, $i = 1, \dots, m, j = 1, \dots, p$. Moment statistics are widely used in point process modeling, especially for a stationary process. For example, the second-order statistic of a univariate point process characterizes the correlation of neighboring locations in a spatial domain (Guan, 2008) or a temporal domain (Guan, 2011), whereas the cross-covariance of a multivariate

point process also characterizes the association between different individual processes (Chen et al., 2019b) additionally.

Conditional intensity function is another crucial quantity, and has been extensively used for modeling both spatial and temporal point processes with additional predictors. For example, consider two temporal point processes $\mathbf{X}(t)$ and $\mathbf{Y}(t)$. Let \mathcal{H}_t^x denote the σ -field generated by $\{\mathbf{X}(s) : s \leq t\}$, the history of $\mathbf{X}(t)$ up to time t . The corresponding \mathcal{H}_t^x -predictable intensity process $\lambda_i^y(t)$ of the point process $Y_i(t)$ is defined as,

$$\lambda_i^y(t)dt = \Pr \{dY_i(t) = 1 | \mathcal{H}_t^x\}, \quad i = 1, \dots, m.$$

For our proposed multivariate point process regression, we mainly target the conditional intensity function, instead of the moment statistics. We explain in detail this choice in Section 3.1.

2.3 Hawkes process

Hawkes (1971) proposed an important class of mutually self-exciting point process, assuming that the event occurrence of each marginal process is triggered by the historical events of the multivariate process. For an m -dimensional linear Hawkes process, the conditional intensity function of the i th marginal process is formulated as,

$$\lambda_i(t) = \mu_i + \sum_{j=1}^m \sum_{l: t_l^j < t} \omega_{ij}(t - t_l^j), \quad i = 1, \dots, m,$$

where μ_i is the background intensity, $\omega_{ij}(\cdot)$ is a non-negative transferring function, and $\{t_1^j, t_2^j, \dots\}$ are the time points of the past events of the j th marginal process, $i, j = 1, \dots, m$. The transferring function ω_{ij} is usually assumed to be some decay kernels. If the process is stationary, then the first and second-order statistics of the linear Hawkes process are fully linked with the background intensity μ_i and the transferring function ω_{ij} via an integral equation system (Bacry and Muzy, 2016). Hawkes process and its variants have been widely studied in temporal point process modeling, and particularly in neuronal spike trains data analysis.

3 Model

3.1 Multivariate point process regression

We consider a regression model with a p -dimensional predictor process $\mathbf{X}(t)$ and an m -dimensional response process $\mathbf{Y}(t)$. In our motivating example, $\mathbf{X}(t)$ and $\mathbf{Y}(t)$ correspond to the neuronal

spike trains in the two target cortex areas, A1 and V1, respectively, and our goal is to model the association patterns among the neurons between the two areas. We assume the conditional intensity of the i th response process $Y_i(t)$ given the predictor process $\mathbf{X}(t)$ is of the form,

$$\lambda_i^y(t) = \phi \left\{ \mu_i + \sum_{j=1}^p (\omega_{ij} * dX_j)(t) \right\}, \quad i = 1, \dots, m, \quad (1)$$

where $\phi(\cdot)$ is a link function, e.g., a rectifier function $\phi(x) = \max(0, x)$, or a sigmoid function $\phi(x) = e^x / (1 + e^x)$, μ_i is the background intensity, and $\omega_{ij}(\cdot) : \mathbb{R}^+ \mapsto \mathbb{R}$ is the transferring function, $i = 1, \dots, m, j = 1, \dots, p$. Write $\boldsymbol{\mu} = (\mu_1, \dots, \mu_m)^\top \in \mathbb{R}^m$, and $\boldsymbol{\omega} = (\omega_{ij}(\cdot)) \in \mathbb{R}^{m \times p}$. Furthermore, we assume that the transferring function $\omega_{ij}(\cdot)$ models the historical information of the predictor process $\mathbf{X}(t)$ in a convolutional fashion, in that,

$$(\omega_{ij} * dX_j)(t) = \int_0^\infty \omega_{ij}(\Delta) dX_j(t - \Delta). \quad (2)$$

This formulation has been commonly used in the Hawkes process literature (e.g., Hawkes, 1971; Zhou et al., 2013b; Chen et al., 2019b) in that $\mathbf{X}(t) = \mathbf{Y}(t)$. However, in our framework, the predictor $\mathbf{X}(t)$ is not limited to any particular point process, even not necessarily a point process. The convolution in (2) works for any real-valued process, including both continuous-valued stochastic process and fixed-value stimulus process. If $X_j(t)$ is indeed a point process, then the corresponding convolution reduces to $\sum_{l \in \{t_l^j < t\}} \omega_{ij}(t - t_l^j)$, where t_l^j is the time of the event of $X_j(t)$. Moreover, similar to Chen et al. (2019b), we do not enforce $\omega_{ij}(\cdot)$ to be non-negative, and therefore we allow both “exciting” and “inhibiting” effects.

The moment statistics are usually informative in capturing the structure of a point process. However, this may not be true in our setting, which differentiates our solution from those moment-based point process modeling approaches. To further understand this, we next consider a special case of our model (1), when there is a linear relation between $\mathbf{X}(t)$ and $\mathbf{Y}(t)$, in that,

$$\lambda_i^y(t) = \mu_i + \sum_{j=1}^p \{\omega_{ij} * dX_j\}(t), \quad i = 1, \dots, m. \quad (3)$$

We next summarize the first and second-order statistics under this special case.

Proposition 1. *Consider a special case of (1) that $\mathbf{X}(t)$ and $\mathbf{Y}(t)$ satisfying the linear relation (3) and both are stationary. Then the corresponding moment statistics are of the form,*

$$\begin{aligned} \Lambda^y &= \boldsymbol{\mu} + \left\{ \int_0^{+\infty} \boldsymbol{\omega}(\Delta) d\Delta \right\} \Lambda^x, & \mathbf{C}^{yx}(\tau) &= \boldsymbol{\omega}(\tau) \text{Diag}(\Lambda^x) + \boldsymbol{\omega} * \mathbf{V}^{xx}(\tau), & \tau \geq 0 \\ \mathbf{V}^{yy}(\tau) &= \boldsymbol{\omega} * \mathbf{C}^{xy}(\tau), & \tau > 0, & \mathbf{V}^{yy}(0) &= \boldsymbol{\omega} \star \{ \mathbf{V}^{xx}(\cdot) + \text{Diag}(\Lambda^x) \} \star \boldsymbol{\omega}, \end{aligned} \quad (4)$$

where $\boldsymbol{\omega} * \mathbf{C}^{xy}(\tau) = \omega_{ij}(\cdot) * C_{ji}^{xy}(\tau)$, and $f * g(t) = \int f(\Delta)g(t - \Delta)d\Delta$ denotes the convolution of two univariate functions f and g , and $\boldsymbol{\omega} \star \{ \mathbf{V}^{xx}(\cdot) + \text{Diag}(\Lambda^x) \} \star \boldsymbol{\omega} = \int_0^{+\infty} \int_0^{+\infty} \boldsymbol{\omega}(\Delta) \{ \text{Diag}(\Lambda^x) \delta(\Delta' - \Delta) + \mathbf{V}^{xx}(\Delta' - \Delta) \} \boldsymbol{\omega}^\top(\Delta') d\Delta d\Delta'$.

The equations in (4) belong to a class of integral equations for the Wiener-Hopf system with respect to $\boldsymbol{\omega}$, analogous to that for a regular Hawkes process (Bacry and Muzy, 2016). Hence, the transferring function can be estimated by solving the above equations and plugging in the empirically estimated first and second-order statistics of $\mathbf{X}(t)$ and $\mathbf{Y}(t)$. However, we argue that moment-based estimation is not suitable for our model, for several reasons. First, moment-based estimation is straightforward when the dimension of the point process is low, but could be challenging when the dimension is high and diverging. Second, compared to a multivariate Hawkes process, the relationship between the moment statistics and the transferring function $\boldsymbol{\omega}$ as shown in (4) is much more complicated. For a Hawkes process, the second-order statistic fully captures the association patterns between the marginal processes. Henceforth, analysis can be carried out without estimating the transferring function. In our model, however, the second-order statistics \mathbf{V}^{yy} and \mathbf{C}^{yx} also depend on the cross-covariance structure of the predictor process $\mathbf{X}(t)$. Third, nearly all moment-based estimation approaches require both the linear form in the conditional intensity function and the stationary condition. These conditions can be restrictive in practice. For these reasons, we choose to adopt an intensity-based modeling approach, instead of a moment-based one. Moreover, we require neither the linear form nor the stationary condition.

3.2 Low-rank structure

In our model, the transferring function $\boldsymbol{\omega}$ fully captures the causal association patterns between the two multivariate processes $\mathbf{X}(t)$ and $\mathbf{Y}(t)$ that is of our interest. Next we assume that $\omega_{ij}(t)$ takes the form of a linear combination of a set of basis effect functions, $g^{(k)}(t)$, $k = 1, \dots, K$, in that,

$$\omega_{ij}(t) = \sum_{k=1}^K \beta_{ij}^k \cdot g^{(k)}(t), \quad i = 1, \dots, m, \quad j = 1, \dots, p, \quad (5)$$

where each $g^{(k)}(t)$ is a non-negative basis function on $[0, \infty)$, K is the number of basis functions, and β_{ij}^k 's can take both positive and negative values. Basis functions are commonly used in point

process modeling (Luo et al., 2016). The choice of basis functions mostly relies on the scientific knowledge (Hansen et al., 2015). In neuronal spike trains study, some common basis functions include the exponential function, $g(t) = a \exp(-at)$, $a > 0$ (Hawkes, 1971; Zhou et al., 2013b), the logarithmic decay function, $g(t) = \log(1 + T - t)$, for the process defined on $[0, T]$ (Luo et al., 2016), and the piecewise constant function, $g_l(t) = a_l \mathbf{1}(t \in \mathcal{T}_l)$, where $\{\mathcal{T}_l\}_{l=1}^L$ form a partition of $[0, +\infty]$ and $\{a_l\}_{l=1}^L$ are some non-negative constants (Wang et al., 2016). One may use one type of basis functions, or a mixture of different types of basis functions.

Given the basis expansion in (5), the conditional intensity model in (1) can be rewritten as,

$$\lambda_i^y(t) = \phi \left[\mu_i + \sum_{j=1}^p \sum_{k=1}^K \beta_{ij}^k \cdot \{g^{(k)} * dX_j\}(t) \right], \quad i = 1, \dots, m. \quad (6)$$

We then collect the transferring coefficients into a three-way tensor $\mathcal{B} \in \mathbb{R}^{m \times p \times K}$, with the entry β_{ij}^k , $i = 1, \dots, m$, $j = 1, \dots, p$, $k = 1, \dots, K$. The conditional intensity function is now fully characterized by the background intensity vector $\boldsymbol{\mu}$ and the transferring coefficient tensor \mathcal{B} .

Next, we impose that \mathcal{B} admits a low-rank CANDECOMP/PARAFAC (CP) structure, in that,

$$\mathcal{B} = \sum_{r=1}^R \nu_r \mathbf{b}_r^y \circ \mathbf{b}_r^x \circ \mathbf{b}_r^c, \quad (7)$$

where R is the tensor rank, $\mathbf{b}_r^y \in \mathbb{R}^m$, $\mathbf{b}_r^x \in \mathbb{R}^p$ and $\mathbf{b}_r^c \in \mathbb{R}^K$ are the normalized vectors corresponding to the modes of the response process, the predictor process, and the convolutional basis functions, respectively, and \circ is the outer product. For notational convenience, we represent the decomposition (7) by a shorthand, $\mathcal{B} = [\boldsymbol{\nu}; \mathbf{B}^y, \mathbf{B}^x, \mathbf{B}^c]$, where $\mathbf{B}^y = [\mathbf{b}_1^y \dots \mathbf{b}_R^y] \in \mathbb{R}^{m \times R}$, $\mathbf{B}^x = [\mathbf{b}_1^x \dots \mathbf{b}_R^x] \in \mathbb{R}^{p \times R}$, $\mathbf{B}^c = [\mathbf{b}_1^c \dots \mathbf{b}_R^c] \in \mathbb{R}^{K \times R}$, and $\boldsymbol{\nu} = (\nu_1, \dots, \nu_R)^\top \in \mathbb{R}^R$. See Kolda and Bader (2009) for a review of tensor and its decomposition. The low-rank decomposition such as (7) has been widely adopted in recent years in imaging-based tensor regressions (Zhou et al., 2013a; Sun and Li, 2017; Chen et al., 2019a). In the context of point process modeling, a similar structure as (7) was first introduced by Zhou et al. (2013b) to model social infection network, and was further studied by Bacry et al. (2015). However, both works assumed a linear intensity function which can be restrictive in practice. Moreover, they only considered a single basis function, and the resulting \mathcal{B} is a matrix. While tensor is a conceptual generalization of matrix, matrix decomposition and tensor decomposition are considerably different (Kolda and Bader, 2009). We also briefly remark that, there are easy-to-check sufficient conditions to ensure the decomposition in (7) is unique up to permutations (Sidiropoulos and Bro, 2000).

Imposing a low-rank structure like (7) in our point process regression has several advantages. First, it substantially reduces the number of free parameters in the transferring coefficient tensor \mathcal{B} , from mpK to $R(m + p + K)$. In our motivation example, the dimensions of response and predictor processes are $m = 139$ and $p = 283$. If we choose $K = 3$ basis functions, and choose the rank $R = 4$, then the number of free parameters in \mathcal{B} reduces from 118,011 to 1,700. Second, and perhaps more importantly, it allows modeling of multivariate point processes in a joint fashion. Nearly all existing intensity-based point process modeling approaches estimate the transferring coefficients in each marginal intensity function $\lambda_i^y(t)$ separately. As such, only the information from a single response process $Y_i(t)$ is utilized, which can be inefficient. By contrast, our method with a decomposition of \mathcal{B} as in (7) essentially suggests the association structures between the individual point processes, both among response processes, and across response and predictor responses, rely on a small number of underlying latent and interrelated factors. In the context of neuronal spike trains modeling, it implies that a particular predictor neuron in $\mathbf{X}(t)$ exercises similar influence on multiple response neurons in $\mathbf{Y}(t)$, or a particular response neuron in $\mathbf{Y}(t)$ enjoys similar influence from multiple predictor neurons in $\mathbf{X}(t)$. Instead of modeling each response $Y_i(t)$ separately, our model allows integration of information across different response and predictor processes.

3.3 Additional structure pursuit: sparsity and subgrouping

To better accommodate scientific knowledge, improve the interpretation, and further reduce the number of free parameters, we consider some additional structure pursuit.

The first structure we pursue is sparsity, in that only a subset of response processes are affected by a subset of predictor processes. This sparsity structure simplifies the model interpretation, further reduces the number of parameters, and is scientifically plausible. In multivariate Hawkes point process modeling, the sparsity on transferring functions has been widely employed (Zhou et al., 2013b; Bacry et al., 2015; Hansen et al., 2015). Specifically, we impose a group Lasso penalty (Yuan and Lin, 2006) on the coefficient tensor \mathcal{B} ,

$$p_s(\mathcal{B}; \tau_s) = \tau_s \sum_{i=1}^m \sum_{j=1}^p \|\mathcal{B}[i, j, \cdot]\|_2, \quad (8)$$

where $\mathcal{B}[i, j, \cdot] \in \mathbb{R}^R$ is a vector of \mathcal{B} with the first two indices fixed and the third index varying that corresponds to the associations between $Y_i(t)$ and $X_j(t)$, τ_s is the sparsity tuning parameter, and $\|\cdot\|_2$ is the L_2 norm.

The second structure we pursue is subgrouping. In neuroscience as well as numerous other applications, the behaviors of multivariate response and predictor variables are often clustered. In a neuronal spike trains study, this clustering phenomenon is usually of great scientific interest (Kim et al., 2011). That is, subsets of neurons are expected to share similar patterns in neuronal firing activities. Such a pattern is reflected by the underlying clustering structure in the transferring function ω . To capture this structure, we embed clustering pursuit into the proposed tensor decomposition. In principle, we can pursue clustering in the response process, or the predictor process, or both. For our motivating example, there is evidence of neuron clustering in the primary visual cortex V1, i.e., our response process (Liang et al., 2013). As such, we introduce a grouping penalty on the decomposed factors of the response mode \mathbf{B}^y , so to encourage clustering of the response neurons. Specifically, we impose a pairwise fusion penalty,

$$p_f(\mathbf{B}^y; \tau_f) = \sum_{i < i'} f_\kappa(\|\mathbf{B}^y[i, \cdot] - \mathbf{B}^y[i', \cdot]\|_2, \tau_f), \quad (9)$$

where $\mathbf{B}^y[i, \cdot] \in \mathbb{R}^R$ is the row vector of \mathbf{B}^y , τ_f is the fusion parameter, and the penalty function $f_\kappa(t, \tau) = \tau \int_0^t \{1 - x/(\tau\kappa)\}_+ dx$, with κ being a thresholding parameter (Zhang et al., 2010). This penalty function is to help reduce the estimation bias, as it only groups the individual predictors with similar effects on the responses through a non-convex fusion penalty (Zhu et al., 2019).

4 Estimation

4.1 ADMM optimization

We develop a highly scalable ADMM type optimization algorithm (Boyd et al., 2011) to estimate the parameters in our proposed model. Consider the realizations of the predictor and response processes $\mathbf{X}(t)$ and $\mathbf{Y}(t)$ on a time interval $[0, T]$. Let $t_1^i < t_2^i < \dots < t_{n_i}^i$ denote the time points of the n_i events of the response process $Y_i(t)$ that are observed on $[0, T]$, $i = 1, \dots, m$. The log-likelihood function for our model is,

$$\begin{aligned} \mathcal{L}(\boldsymbol{\mu}, \mathbf{B}) &= -\frac{1}{T} \sum_{i=1}^m L_i(\boldsymbol{\mu}, \mathbf{B}) \equiv -\frac{1}{T} \sum_{i=1}^m \int_0^T \left[\log \{\lambda_i^y(t)\} dY_i(t) - \lambda_i^y(t) dt \right] \\ &= \frac{1}{T} \sum_{i=1}^m \left(\int_0^T \phi \{ \mu_i + \langle \mathbf{G}(t), \mathbf{B}[i, \cdot, \cdot] \rangle \} dt - \sum_{l=1}^{n_i} \log [\phi \{ \mu_i + \langle \mathbf{G}(t_l^i), \mathbf{B}[i, \cdot, \cdot] \rangle \}] \right), \end{aligned} \quad (10)$$

where $\mathbf{G}(t) = (G_{j,k}(t)) \in \mathbb{R}^{p \times K}$, $G_{j,k}(t) = \{g^{(k)} * dX_j\}(t)$, $\mathbf{B}[i, \cdot, \cdot] \in \mathbb{R}^{p \times K}$ is a matrix from \mathbf{B} with the first index fixed and the other two indices varying, and $\langle \cdot, \cdot \rangle$ denotes the inner product.

Incorporating the low-rank structure (7) and the two regularization structures (8) and (9), we aim at the following optimization problem,

$$\min_{\boldsymbol{\mu}, \boldsymbol{\nu}, \mathbf{B}^y, \mathbf{B}^x, \mathbf{B}^c} \left\{ \mathcal{L}(\boldsymbol{\mu}, \llbracket \boldsymbol{\nu}; \mathbf{B}^y, \mathbf{B}^x, \mathbf{B}^c \rrbracket) + \tau_s \sum_{i=1}^m \sum_{j=1}^p \left\| \llbracket \boldsymbol{\nu}; \mathbf{B}^y, \mathbf{B}^x, \mathbf{B}^c \rrbracket [i, j, \cdot] \right\|_2 \right. \\ \left. + \sum_{i < i'} f_\kappa \left(\left\| \mathbf{B}^y [i, \cdot] - \mathbf{B}^y [i', \cdot] \right\|_2, \tau_f \right) \right\}. \quad (11)$$

The optimization in (11) is challenging in several ways. It involves a tensor decomposition embedded in a complicated log-likelihood function with summation of integrals and a possibly nonlinear link function ϕ . In addition, the sparsity penalty in (8) is non-differentiable, while the fusion penalty in (9) is non-convex. Moreover, (9) involves the differences of parameters, rendering those parameters inseparable in optimization. To overcome those challenges, and to achieve computational scalability, we develop an ADMM algorithm for the optimization in (11).

Specifically, we introduce three sets of auxiliary variables. The first set is $\mathcal{A} \in \mathbb{R}^{m \times p \times K}$ that targets the low-rank structure (7) such that $\mathcal{A} = \mathcal{B} = \llbracket \boldsymbol{\nu}; \mathbf{B}^y, \mathbf{B}^x, \mathbf{B}^c \rrbracket$. The second set is $\Psi \in \mathbb{R}^{m \times p \times K}$ with $\Psi [i, j, \cdot] = \boldsymbol{\psi}_{ij} \in \mathbb{R}^K$ that targets the sparsity structure (8) such that $\boldsymbol{\psi}_{ij} = \mathcal{B} [i, j, \cdot]$, $1 \leq i \leq m, 1 \leq j \leq p$. The thxrd set is $\Gamma \in \mathbb{R}^{m(m-1)/2 \times R}$ that stacks $\boldsymbol{\gamma}_{ii'} \in \mathbb{R}^R$ together and targets the subgroup structure (9) such that $\boldsymbol{\gamma}_{ii'} = \mathbf{B}^y [i, \cdot] - \mathbf{B}^y [i', \cdot]$, $1 \leq i < i' \leq m$. We then rewrite (11) in its equivalent form,

$$\min_{\boldsymbol{\mu}, \boldsymbol{\nu}, \mathbf{B}^y, \mathbf{B}^x, \mathbf{B}^c, \mathcal{A}, \Psi, \Gamma} \left\{ \mathcal{L}(\boldsymbol{\mu}, \mathcal{A}) + \tau_s \sum_{i=1}^m \sum_{j=1}^p \left\| \boldsymbol{\psi}_{ij} \right\|_2 + \sum_{j < j'} f_\kappa \left(\left\| \boldsymbol{\gamma}_{ii'} \right\|_2, \tau_f \right) \right\} \\ \text{subject to } \mathcal{A} = \llbracket \boldsymbol{\nu}; \mathbf{B}^y, \mathbf{B}^x, \mathbf{B}^c \rrbracket, \quad \Psi = \mathcal{B}, \quad \Gamma = \mathbf{D}_m \mathbf{B}^y, \quad (12)$$

where $\mathbf{D}_m \in \mathbb{R}^{m(m-1)/2 \times m}$ that stacks $\mathbf{d}_{ii'} \in \mathbb{R}^m$ together, with $\mathbf{d}_{ii'} = \mathbf{e}_i - \mathbf{e}_{i'}$, $\mathbf{e}_i \in \mathbb{R}^m$ has one on the i th position and zero elsewhere, $1 \leq i < i' \leq m$. Note that the second constraint $\Psi = \mathcal{B}$ can also be written as $\Psi = \mathcal{A}$ due to the first constraint. To solve (12), we minimize the following augmented Lagrangian objective function,

$$\mathcal{L}(\mathcal{A}, \boldsymbol{\mu}) + \tau_s \sum_{i,j} \left\| \boldsymbol{\psi}_{ij} \right\|_2 + \sum_{j < j'} f_\kappa \left(\left\| \boldsymbol{\gamma}_{ii'} \right\|_2, \tau_f \right) \\ + \langle \mathcal{W}_1, \mathcal{A} - \llbracket \boldsymbol{\nu}; \mathbf{B}^y, \mathbf{B}^x, \mathbf{B}^c \rrbracket \rangle + \langle \mathcal{W}_2, \Psi - \mathcal{A} \rangle + \langle \mathcal{W}_3, \Gamma - \mathbf{D}_m \mathbf{B}^y \rangle \\ + \frac{\rho}{2} \left(\left\| \mathcal{A} - \llbracket \boldsymbol{\nu}; \mathbf{B}^y, \mathbf{B}^x, \mathbf{B}^c \rrbracket \right\|_F^2 + \left\| \Psi - \mathcal{A} \right\|_F^2 + \left\| \Gamma - \mathbf{D}_m \mathbf{B}^y \right\|_F^2 \right),$$

where $\mathcal{W}_1, \mathcal{W}_2 \in \mathbb{R}^{m \times p \times K}$ and $\mathcal{W}_3 \in \mathbb{R}^{m(m-1)/2 \times m}$ are the corresponding Lagrangian multipliers, $\rho > 0$ is a fixed augmented parameter, and $\| \cdot \|_F$ denotes the Frobenius norm.

Next we update the blocks of parameters, $\boldsymbol{\mu}, \mathcal{A}, \boldsymbol{\nu}, \mathbf{B}^y, \mathbf{B}^x, \mathbf{B}^c, \boldsymbol{\Psi}, \boldsymbol{\Gamma}$, and the Lagrangian multipliers $\mathcal{W}_1, \mathcal{W}_2, \mathcal{W}_3$ in an alternating fashion. That is, given the estimates at the s th iteration, $\mathcal{A}^{(s)}, \mathcal{B}^{(s)} = \llbracket \{\boldsymbol{\nu}\}^{(s)}; \{\mathbf{B}^y\}^{(s)}, \{\mathbf{B}^x\}^{(s)}, \{\mathbf{B}^c\}^{(s)} \rrbracket, \boldsymbol{\Psi}^{(s)}, \boldsymbol{\Gamma}^{(s)}, \mathcal{W}_1^{(s)}, \mathcal{W}_2^{(s)}, \mathcal{W}_3^{(s)}$, we update the parameters at the $(s+1)$ th iteration as,

$$\boldsymbol{\mu}^{(s+1)}, \mathcal{A}^{(s+1)} = \underset{\boldsymbol{\mu}, \mathcal{A}}{\operatorname{argmin}} \mathcal{L}(\mathcal{A}, \boldsymbol{\mu}) + \frac{\rho}{2} \left\{ \left\| \mathcal{A} - \mathcal{B}^{(s)} + \rho^{-1} \mathcal{W}_1^{(s)} \right\|_F^2 + \left\| \mathcal{A} - \boldsymbol{\Psi}^{(s)} + \rho^{-1} \mathcal{W}_2^{(s)} \right\|_F^2 \right\}, \quad (13)$$

$$\mathcal{B}^{(s+1)} = \underset{\boldsymbol{\nu}, \mathbf{B}^y, \mathbf{B}^x, \mathbf{B}^c}{\operatorname{argmin}} \left\| \llbracket \boldsymbol{\nu}; \mathbf{B}^y, \mathbf{B}^x, \mathbf{B}^c \rrbracket - \mathcal{A}^{(s+1)} - \rho^{-1} \mathcal{W}_1^{(s)} \right\|_F^2 + \left\| \boldsymbol{\Gamma}^{(s)} - D_p \mathbf{B}^y - \rho^{-1} \mathcal{W}_3^{(s)} \right\|_F^2, \quad (14)$$

$$\boldsymbol{\Psi}^{(s+1)} = \underset{\boldsymbol{\Psi}}{\operatorname{argmin}} \frac{\rho}{2} \left\| \boldsymbol{\Psi} - \mathcal{A}^{(s+1)} - \rho^{-1} \mathcal{W}_2^{(s)} \right\|_F^2 + \tau_s \sum_{i,j} \|\boldsymbol{\psi}_{ij}\|_2, \quad (15)$$

$$\boldsymbol{\Gamma}^{(s+1)} = \underset{\boldsymbol{\Gamma}}{\operatorname{argmin}} \frac{\rho}{2} \left\| \boldsymbol{\Gamma} - D_p (\mathbf{B}^y)^{(s+1)} - \rho^{-1} \mathcal{W}_3^{(s)} \right\|_F^2 + \sum_{j < j'} f_\rho(\|\boldsymbol{\gamma}_{jj'}\|_2, \tau_f). \quad (16)$$

$$\begin{aligned} \mathcal{W}_1^{(s+1)} &= \mathcal{W}_1^{(s)} + \rho \left\{ \mathcal{A}^{(s+1)} - \mathcal{B}^{(s+1)} \right\}, \\ \mathcal{W}_2^{(s+1)} &= \mathcal{W}_2^{(s)} + \rho \left\{ \mathcal{A}^{(s+1)} - \boldsymbol{\Psi}^{(s+1)} \right\}, \\ \mathcal{W}_3^{(s+1)} &= \mathcal{W}_3^{(s)} + \rho \left\{ D_m (\mathbf{B}^y)^{(s+1)} - \boldsymbol{\Gamma}^{(s+1)} \right\}. \end{aligned} \quad (17)$$

We then tackle the optimization problems (13) to (16) one-by-one.

The optimization problem in (13) can be split slice-by-slice for $\mathcal{A}[i, \cdot, \cdot], i = 1, \dots, m$. That is, it can be solved with respect to each marginal response process $Y_i(t)$ in a parallel fashion. Define

$$\begin{aligned} L_i^*(\mu_i, \mathcal{A}[i, \cdot, \cdot]) &= -\frac{1}{T} \sum_{l=1}^{n_i} \log [\phi \{ \mu_i + \langle \mathbf{G}(t_l^i), \mathcal{A}[i, \cdot, \cdot] \rangle \}] + \frac{1}{T} \int_0^T \phi \{ \mu_i + \langle \mathbf{G}(t), \mathcal{A}[i, \cdot, \cdot] \rangle \} dt \\ &+ \frac{\rho}{2} \left\| \mathcal{A}[i, \cdot, \cdot] - \mathcal{B}^{(s)}[i, \cdot, \cdot] + \rho^{-1} \mathcal{W}_1^{(s)}[i, \cdot, \cdot] \right\|_F^2 + \frac{\rho}{2} \left\| \mathcal{A}[i, \cdot, \cdot] - \boldsymbol{\Psi}^{(s)}[i, \cdot, \cdot] + \rho^{-1} \mathcal{W}_2^{(s)}[i, \cdot, \cdot] \right\|_F^2. \end{aligned}$$

The objective function $L_i^*(\mu_i, \mathcal{A}[i, \cdot, \cdot])$ is differentiable, and with a large enough ρ , it is almost convex regardless of the form of the link function ϕ . Therefore, we can minimize $L_i^*(\mu_i, \mathcal{A}[i, \cdot, \cdot])$ efficiently using a gradient descent type algorithm. In our implementation, we consider the linear and the logit link function ϕ , and corresponding, we employ the Newton-Raphson algorithm to minimize $L_i^*(\mu_i, \mathcal{A}[i, \cdot, \cdot])$.

The optimization problem in (14) turns to be a regularized CP decomposition with an L_2 penalty. It can be solved by an alternating block updating algorithm (Zhou et al., 2013a). That

is, we alternately update one block of the parameters in $\{\mathbf{B}^y, \mathbf{B}^x, \mathbf{B}^c\}$, while fixing the other two blocks and $\boldsymbol{\nu}$. For instance, \mathbf{B}^y is updated by minimizing the following objective,

$$\min_{\mathbf{B}^y} \left\| \left\{ \mathcal{A}^{(s+1)} + \rho^{-1} \mathcal{W}_1^{(s)} \right\}_{(1)} - \mathbf{B}^y [(\mathbf{B}^c)^{(s)} \odot (\mathbf{B}^x)^{(s)} \text{diag}\{\boldsymbol{\nu}^{(s)}\}]^\top \right\|^2 + \left\| \boldsymbol{\Gamma}^{(s)} - \rho^{-1} \mathcal{W}_3^{(s)} - \mathbf{D}_m \mathbf{B}^y \right\|^2,$$

with respect to \mathbf{B}^y , where \odot is the Khatri-Rao product of two matrices, $\mathcal{A}_{(1)}$ denotes the mode-1 matricization of the tensor \mathcal{A} , and $\text{diag}(\boldsymbol{\nu})$ is the diagonal matrix with $\boldsymbol{\nu}$ as the diagonal elements. Note that this is essentially a least squares optimization problem with an L_2 penalty, which has an explicit solution. The other two blocks \mathbf{B}^x and \mathbf{B}^c are updated similarly, by dropping the second term in the above objective function, and the problem becomes a least squares optimization. After updating each block, for instance, \mathbf{B}^y , we update ν_r by normalizing the corresponding vector \mathbf{b}_r^y , $r = 1, \dots, R$, respectively. In addition, we employ the maximum block improvement strategy of Chen et al. (2012) to ensure the convergence of the alternating block updating iterations.

The optimization problems in (15) and (16) have explicit solutions, since the corresponding objective functions are convex with respect to ψ_{ij} , and $\gamma_{ii'}$ when $\kappa > \rho^{-1}$, respectively. That is,

$$\psi_{ij}^{(s+1)} = \begin{cases} \mathbf{0} & \text{if } \|\boldsymbol{\vartheta}_{ij}^{(s+1)}\| < \sqrt{K} \tau_s / \rho, \\ \left\{ 1 - \frac{\sqrt{K} \tau_s / \rho}{\|\boldsymbol{\vartheta}_{ij}^{(s+1)}\|} \right\} \boldsymbol{\vartheta}_{ij}^{(s+1)} & \text{if } \|\boldsymbol{\vartheta}_{ij}^{(s+1)}\| \geq \sqrt{K} \tau_s / \rho, \end{cases} \quad (18)$$

where $\boldsymbol{\vartheta}_{ij}^{(s+1)} = \mathcal{A}[i, j, \cdot]^{(s+1)} + \rho^{-1} \{\mathcal{W}_2[i, j, \cdot]\}^{(s)}$. We note that this computation can be done in a parallel fashion again over $(i, i'), 1 \leq i, i' \leq m$, and $(i, j), i = 1, \dots, m, j = 1, \dots, p$;

$$\gamma_{ii'}^{(s+1)} = \begin{cases} \zeta_{ii'}^{(s+1)} & \text{if } \|\zeta_{ii'}^{(s+1)}\| \geq \kappa \tau_f, \\ \frac{\kappa \rho}{\kappa \rho - 1} \left\{ 1 - \frac{\tau_f / \rho}{\|\zeta_{ii'}^{(s+1)}\|} \right\}_+ \zeta_{ii'}^{(s+1)} & \text{if } \|\zeta_{ii'}^{(s+1)}\| < \kappa \tau_f, \end{cases} \quad (19)$$

where $\zeta_{ii'}^{(s+1)} = (\mathbf{B}^y[i, \cdot])^{(s+1)} - (\mathbf{B}^y[i', \cdot])^{(s+1)} + \rho^{-1} \mathcal{W}_3[l_{ii'}, \cdot]^{(s)}$, and $l_{ii'} = (2m - i)(i - 1) / 2 + i' - i$, $1 \leq i < i' \leq m$.

We summarize the above optimization procedures in Algorithm 1.

4.2 Initialization, convergence, and tuning

We recommend to use a warm initialization, by setting the initial values $\{\boldsymbol{\mu}^{(0)}, \mathcal{B}^{(0)}\}$ as the unpenalized estimators without imposing any low-rank or penalty structures, while setting the other

Algorithm 1 The ADMM algorithm for parameter estimation.

- [1] Initialize $\boldsymbol{\mu}^{(0)}, \llbracket \boldsymbol{\nu}; \mathbf{B}^y, \mathbf{B}^x, \mathbf{B}^c \rrbracket^{(0)}, \mathcal{A}^{(0)}, \boldsymbol{\Psi}^{(0)}, \boldsymbol{\Gamma}^{(0)}, \mathcal{W}_1^{(0)}, \mathcal{W}_2^{(0)}, \mathcal{W}_3^{(0)}$. Set ρ and $\kappa > \rho^{-1}$.
repeat
 [2] Update $\boldsymbol{\mu}_i^{(s+1)}, \mathcal{A}[i, \cdot, \cdot]^{(s+1)}$ via (13) with parallel computing over $i = 1, \dots, m$.
 [3] Update $\llbracket \boldsymbol{\nu}^{(s+1)}; \{\mathbf{B}^y\}^{(s+1)}, \{\mathbf{B}^x\}^{(s+1)}, \{\mathbf{B}^c\}^{(s+1)} \rrbracket$ via (14).
 [4] Update $\boldsymbol{\Psi}^{(s+1)} = \{\boldsymbol{\psi}_{ij}^{(s+1)}\}$ via (18) with parallel computing over $1 \leq i \leq m, 1 \leq j \leq p$.
 [5] Update $\boldsymbol{\Gamma}^{(s+1)} = \{\boldsymbol{\gamma}_{ii'}^{(s+1)}\}$ via (19) with parallel computing over $1 \leq i < i' \leq m$.
 [6] Update $\mathcal{W}_1^{(s+1)}, \mathcal{W}_2^{(s+1)}, \mathcal{W}_3^{(s+1)}$ via (17).
until the stopping criterion is met.
-

initial values at zeros. We stop the algorithm when the following stopping criterion is met; i.e.,

$$\frac{1}{mpK} \|\mathcal{A}^{(s+1)} - \mathcal{A}^{(s)}\|^2 + \frac{1}{m} \|\boldsymbol{\mu}^{(s+1)} - \boldsymbol{\mu}^{(s)}\|^2 < 10^{-3}, \quad \text{and}$$

$$\frac{1}{mpK} \|\mathcal{R}_1^{(s+1)} - \mathcal{R}_1^{(s)}\|^2 + \frac{1}{mpK} \|\mathcal{R}_2^{(s+1)} - \mathcal{R}_2^{(s)}\|^2 + \frac{2}{m^2(m-1)} \|\mathcal{R}_3^{(s+1)} - \mathcal{R}_3^{(s)}\|^2 < 10^{-3},$$

where $\mathcal{R}_1^{(s)} = \mathcal{A}^{(s)} - \mathcal{B}^{(s)}$, $\mathcal{R}_2^{(s)} = \boldsymbol{\Psi}^{(s)} - \mathcal{A}^{(s)}$, and $\mathcal{R}_3^{(s)} = \boldsymbol{\Gamma}^{(s)} - \mathbf{D}_m(\mathbf{B}^y)^{(s)}$.

Algorithm 1 converges to a stationary point (Tang et al., 2019). This can be verified by checking the conditions of Proposition 1 in Zhu et al. (2019) and Theorem 1 in Wang et al. (2019).

Proposition 2. *Suppose the log-likelihood function \mathcal{L} is a Lipschitz function with respect to \mathcal{B} , and the parameter space for \mathbf{B}^y , \mathbf{B}^x and \mathbf{B}^c is a compact set. Then the obtained estimator from Algorithm 1 converges to a stationary point of the objective function in (11).*

We select the tuning parameters as follows. The first is the Lagrangian augmented parameter ρ , which can be viewed as the learning rate of the ADMM algorithm. Our numerical results have suggested that the final estimates are not overly sensitive to the choice of ρ , so we simply set $\rho = 1$. The second is the thresholding parameter κ in the fusion penalty f_κ . Again, the estimates are not sensitive to κ as long as $\kappa > \rho^{-1}$, and we set $\kappa = 2$. The third set of tuning parameters include the rank R in (7), and the two regularization parameters, τ_s in (8) and τ_f in (9). We tune them by minimizing a Bayesian information criterion (BIC), $-2\mathcal{L}(\boldsymbol{\mu}, \mathcal{B}) + \log(N)p_e$, where $N = \sum_{i=1}^m n_i$ is the total number of events observed on the multivariate response process $\mathbf{Y}(t)$, and p_e is the effective number of parameters. For the tuning of R , $p_e = R(m + p + K - 2)$, for τ_s , p_e is the total number of non-zero latent parameters, and for τ_f , p_e is the total number of unique non-zero latent parameters. A similar BIC type criterion has been commonly adopted in low-rank tensor

regressions (Zhou et al., 2013a; Sun and Li, 2017). Moreover, to speed up tuning, we tune R, τ_s, τ_f in a sequential manner. That is, we first tune R while setting $\tau_s = \tau_f = 0$, then tune τ_s given the selected R while setting $\tau_f = 0$, and finally tune τ_f given the selected R and τ_s .

5 Theory

5.1 Regularity conditions and supporting lemmas

We first present a set of regularity conditions, and three lemmas that are useful to establish the theoretical properties.

We begin by introducing a set of notations. Let $\boldsymbol{\theta} = \{\boldsymbol{\mu}^\top, \text{vec}(\mathbf{B}^y)^\top, \text{vec}(\mathbf{B}^x)^\top, \text{vec}(\mathbf{B}^c)^\top\}^\top$ collect all the parameters of interest in our model, including the background intensity $\boldsymbol{\mu}$ and the latent factors $\mathbf{B}^y, \mathbf{B}^x, \mathbf{B}^c$ from the CP decomposition (7). Since $\boldsymbol{\nu}$ in (7) is obtained from the normalization, it is omitted to simplify the notation. Let $\boldsymbol{\beta} = (\boldsymbol{\beta}_1^\top, \dots, \boldsymbol{\beta}_m^\top)^\top$, where $\boldsymbol{\beta}_i = \{\mu_i, \text{vec}(\mathcal{B}[i, \cdot, \cdot])^\top\}^\top$, $i = 1, \dots, m$. Note that $\boldsymbol{\beta}$ is a function of $\boldsymbol{\theta}$, but is useful in our theoretical derivations, since the evaluation of the likelihood function is through $\boldsymbol{\mu}$ and \mathcal{B} . Let $\Theta_\theta \subset \mathbb{R}^{R(m+p+K)+m}$ and $\Theta_\beta \subset \mathbb{R}^{mpK+m}$ denote the parameter space for $\boldsymbol{\theta}$ and $\boldsymbol{\beta}$, respectively. For a real-valued function $f(t)$ defined on $[0, \infty)$, define the norm $\|f\|_A = \{\int_A f^2(s)ds\}^{1/2}$, where A is a Borel set in $[0, \infty]$. In particular, write $\|f\|_t = \{\int_0^t f^2(s)ds\}^{1/2}$. Moreover, let $\|\cdot\|_2, \|\cdot\|_\infty, \|\cdot\|_F$, and $\|\cdot\|_{max}$ denote the L_2 norm, the L_∞ norm, the Frobenius norm, and the maximum norm, respectively. Let $\pi_{min}(\cdot)$ and $\pi_{max}(\cdot)$ denote the smallest and the largest eigenvalue for a symmetric matrix. Let \mathcal{H}_t denote the σ -algebra generated by $\{\mathbf{X}(t), \mathbf{Y}(t)\}$. Then the intensity function of $\mathbf{Y}(t)$ as defined in (1) is an \mathcal{H}_t -predictable process.

We consider a general class of link functions and penalty functions for the asymptotic study, which encompass our model (1) and the two penalty functions (8) and (9). Specifically, consider

$$\mathcal{S}(\boldsymbol{\theta}) = \mathcal{L}(\boldsymbol{\theta}) + \tau p(\boldsymbol{\theta}) = -\frac{1}{T} \sum_{i=1}^m L_i(\boldsymbol{\theta}) + \tau p(\boldsymbol{\theta}), \quad (20)$$

where \mathcal{L} and L_i , $i = 1, \dots, m$, are the log-likelihood functions as defined in (10), $p(\cdot)$ is a non-negative penalty function, and τ is the penalization parameter. Note that the unknown latent parameter $\boldsymbol{\theta}$ is associated with the intensity function $\lambda_i^y(t)$ and the log-likelihood function L_i through $\boldsymbol{\beta}$. Henceforth, both $\lambda_i^y(t)$ and L_i are functions of $\boldsymbol{\beta}$. For notational simplicity, we sometimes drop $\boldsymbol{\beta}$ in $\lambda_i^y(t)$ and L_i . We denote $\dot{\lambda}_i^y(t) = \partial \lambda_i^y(t) / \partial \boldsymbol{\beta}_i \in \mathbb{R}^{pK \times 1}$, $\ddot{\lambda}_i^y(t) = \partial^2 \lambda_i^y(t) / \partial \boldsymbol{\beta}_i \partial \boldsymbol{\beta}_i^\top \in \mathbb{R}^{pK \times pK}$,

and $\mathbf{H}_i(t) = \lambda_i^y(t)^{-1} \dot{\lambda}_i^y(t) \in \mathbb{R}^{pK \times 1}$, which are all \mathcal{H}_t -predictable processes. We denote

$$\begin{aligned}\dot{\mathbf{L}}_i &= -\frac{1}{T} \frac{\partial L_i}{\partial \boldsymbol{\beta}_i} = \frac{1}{T} \int_0^T \mathbf{H}_i(t) \{ \lambda_i^y(t) dt - dY_i(t) \} \in \mathbb{R}^{pK \times 1}, \\ \ddot{\mathbf{L}}_i &= -\frac{1}{T} \frac{\partial^2 L_i}{\partial \boldsymbol{\beta}_i \partial \boldsymbol{\beta}_i^\top} = \frac{1}{T} \int_0^T \left[\ddot{\lambda}_i^y(t) dt + \left\{ \mathbf{H}_i(t) \mathbf{H}_i(t)^\top - \lambda_i^y(t)^{-1} \dot{\lambda}_i^y(t) \right\} dY_i(t) \right] \in \mathbb{R}^{pK \times pK}.\end{aligned}$$

It is clear that each set of parameters $\boldsymbol{\beta}_i$ is only involved in the marginal likelihood function for the i th response process. We write the gradient $\dot{\mathbf{L}} = \partial \mathcal{L} / \partial \boldsymbol{\beta} = \left(\dot{\mathbf{L}}_1^\top, \dots, \dot{\mathbf{L}}_m^\top \right)^\top \in \mathbb{R}^{mpK \times 1}$, and the Hessian matrix $\ddot{\mathbf{L}} = \partial^2 \mathcal{L} / \partial \boldsymbol{\beta} \partial \boldsymbol{\beta}^\top = \text{diag} \left(\ddot{\mathbf{L}}_1, \dots, \ddot{\mathbf{L}}_m \right) \in \mathbb{R}^{mpK \times mpK}$. Let $\boldsymbol{\theta}^0, \boldsymbol{\beta}^0$ and $\lambda_i^0(t) = \lambda_i^y(t, \boldsymbol{\beta}^0)$ denote the true values for $\boldsymbol{\theta}, \boldsymbol{\beta}$ and $\lambda_i^y(t)$, respectively. Furthermore, we denote

$$\mathbf{J}_i = \frac{1}{T} \int_0^T \mathbf{H}_i(t) \mathbf{H}_i(t)^\top \lambda_i^0(t) dt \in \mathbb{R}^{pK \times pK}, \quad \text{and } \mathbf{J} = \text{diag}(\mathbf{J}_1, \dots, \mathbf{J}_m) \in \mathbb{R}^{mpK \times mpK}.$$

One can show that $\mathbf{J}_i(\boldsymbol{\beta}^0) = \mathbb{E}\{\ddot{\mathbf{L}}_i(\boldsymbol{\beta}^0)\} = T \text{Var}\{\dot{\mathbf{L}}_i(\boldsymbol{\beta}^0)\}$, and thus $\mathbf{J}(\boldsymbol{\beta}^0) = \mathbb{E}\{\ddot{\mathbf{L}}(\boldsymbol{\beta}^0)\} = T \text{Var}\{\dot{\mathbf{L}}(\boldsymbol{\beta}^0)\}$, which is simply the Fisher information matrix. Again we express the corresponding functions of $\boldsymbol{\beta}^0$ explicitly, and drop $\boldsymbol{\beta}^0$ for notational simplicity when there is no confusion.

Next, we introduce the regularity conditions. Most existing theoretical studies of point process modeling assume a stationary process, a linear intensity function, or a fixed dimensionality. We however do not impose any of those conditions. Instead, we place some relatively mild conditions on the intensity function, the link function, and the basis function.

(A1) The parameter space Θ_θ is compact, that is, there exists a finite positive constant c_0 , such that, $\|\boldsymbol{\theta}\|_\infty \leq c_0$ for any $\boldsymbol{\theta} \in \Theta_\theta$.

(A2) There exist finite positive constants $c_1, c'_1, c_1^*, c_2, c_2^*$, such that, for any $\boldsymbol{\beta} \in \Theta_\beta$ and $t > 0, 0 < c'_1 \leq \min_{1 \leq i \leq m} \lambda_i^y(t) \leq \max_{1 \leq i \leq m} \lambda_i^y(t) \leq c_1$ and $\max_{1 \leq i \leq m} \sup_{\mathcal{V}(A) < 1} \mathbb{E}\{Y_i(A)\}^2 / \mathcal{V}(A) \leq c_1^*$, where A is a Borel-set on $[0, +\infty)$ and \mathcal{V} denotes the Lesbegue measure. Similarly, $\max_{1 \leq j \leq p} \lambda_j^x(t) \leq c_2$ and $\max_{1 \leq j \leq p} \sup_{\mathcal{V}(A) < 1} \mathbb{E}\{X_j(A)\}^2 / \mathcal{V}(A) \leq c_2^*$, where $\lambda_j^x(t)$ is the conditional intensity function of the predictor process $X_j(t), j = 1, \dots, p$.

(A3) There exist finite positive constants c_3, c_4, c_5 , such that, for any $\boldsymbol{\beta} \in \Theta_\beta$ and $t > 0, \max_{1 \leq i \leq m} \|\dot{\lambda}_i^y(t)\|_\infty \leq c_3, \max_{1 \leq i \leq m} \|\ddot{\lambda}_i^y(t)\|_{max} \leq c_4$, and $\max_{1 \leq i \leq m, 1 \leq l_1, l_2, l_3 \leq pK} |\partial^3 \lambda_i^y(t) / \partial \beta_{i, l_1} \partial \beta_{i, l_2} \partial \beta_{i, l_3}| \leq c_5$, almost surely, where β_{i, l_s} denotes the l_s th element of $\boldsymbol{\beta}_i$.

(A4) There exists a finite positive constant c_6 and some large $T_1 > 0$, such that, for any $T > T_1$ and $\boldsymbol{\beta} \in \Theta_\beta, \min_{1 \leq i \leq m} \pi_{min}(\mathbf{J}_i) > c_6$ almost surely.

- (A5) For $\beta, \tilde{\beta} \in \Theta_\beta$, $\lambda_i^y(t; \beta) = \lambda_i^y(t; \tilde{\beta})$ almost surely, if and only if $\beta = \tilde{\beta}$. Here $\lambda_i^y(t; \beta)$ expresses the intensity $\lambda_i^y(t)$ as a function of β explicitly.
- (A6) The link function $\phi(x)$ is a Lipschitz function satisfying that $|\phi(x_1) - \phi(x_2)| \leq c_7|x_1 - x_2|$, for any $x_1, x_2 \in R$, and some finite positive constant c_7 .
- (A7) The basis functions $g^{(k)}(t), k = 1, \dots, K$, satisfy that $\max_{1 \leq k \leq K} \|g^{(k)}(t)\|_T \leq c_8$, for some positive constant c_8 .
- (A8) The penalty function $p(\theta)$ is a non-negative Lipschitz function in a neighborhood of $\theta^0 \in \Theta_\theta$ satisfying that $|p(\theta_1) - p(\theta_2)| \leq c_9\|\theta_1 - \theta_2\|_2$ for some finite positive constant c_9 .

Assumptions (A2) to (A5) are placed on the intensity function, and are commonly used in asymptotic studies of point process modeling (Ogata et al., 1978; Rathbun and Cressie, 1994; Hansen et al., 2015). Assumption (A2) places bounds on intensity function for both the response process and the predictor process. For the response process, it naturally holds in numerous cases; e.g., when a sigmoid link function is employed, or when the response point process is orderly. Assumption (A3) requires bounded higher-order derivative for the intensity function, which is easy to verify for a class of commonly used link functions. For instance, for an identity link function, we have that $\dot{\lambda}_i = [1, \text{vec}\{\mathbf{G}(t)\}^\top]^\top$, and $\ddot{\lambda}_i^y(t) = \mathbf{0}$. For a sigmoid link function, we have that $\dot{\lambda}_i^y(t) = [\lambda_i^y(t)\{1 - \lambda_i^y(t)\}] [1, \text{vec}\{\mathbf{G}(t)\}^\top]^\top$, and $\ddot{\lambda}_i^y(t) = \{1 - 2\lambda_i^y(t)\}\ddot{\lambda}_i^y(t) [1, \text{vec}\{\mathbf{G}(t)\}^\top]$, which are bounded for all t , as long as $\|\text{vec}\{\mathbf{G}(t)\}\|_2$ is uniformly bounded. Assumption (A4) is placed on the eigenvalues of the information matrix. Assumption (A5) ensures the identifiability of $\lambda_i^y(t)$ with respect to β , and is analogous to Assumption (B3) of Ogata et al. (1978). Assumption (A6) characterizes the smoothness of the link function. Assumption (A7) places bounds for the basis functions, which easily hold for a variety of basis functions, as they are usually some decay kernel functions. Assumption (A8) poses a general condition on the penalty function, which holds for various common penalty functions such as the L_1 and L_2 penalties. Overall, we view the above regularity conditions mild and reasonable.

Next, we present three useful lemmas. The first lemma characterizes the smoothness of the loss function with respect to β , which is crucial to derive the convergence rate of the estimator.

Lemma 1. *Suppose Assumptions (A1), (A5) and (A7) hold. Then, for any $\beta, \tilde{\beta} \in \Theta_\beta$, there exists some finite positive constant c_{10} , such that*

$$\frac{1}{T} \sum_{i=1}^m \left\| \lambda_i^y(t; \boldsymbol{\beta}) - \lambda_i^y(t; \tilde{\boldsymbol{\beta}}) \right\|_T^2 \leq c_7^2 h_x^2 \|\boldsymbol{\beta} - \tilde{\boldsymbol{\beta}}\|_2^2,$$

where h_x is a measurable function of $\mathbf{X}(t)$ on $[0, T]$ such that $\mathbb{E}(h_x^2) \leq (1 + c_{10}pK)$. Here $\lambda_i^y(t; \boldsymbol{\beta})$ expresses $\lambda_i^y(t)$ as a function of $\boldsymbol{\beta}$ explicitly. Moreover, there exist some finite positive constant c_{11} , such that

$$\left| \mathcal{L}(\boldsymbol{\beta}) - \mathcal{L}(\tilde{\boldsymbol{\beta}}) \right| \leq c_7 \sqrt{m} h_x (1 + c_{11} h_y) \|\boldsymbol{\beta} - \tilde{\boldsymbol{\beta}}\|_2,$$

where h_y is a measurable function of $\mathbf{Y}(t)$ on $[0, T]$ such that $\mathbb{E}(h_y^2) \leq c_1^*$.

The second lemma links the coefficients $\boldsymbol{\beta}$ with the parameters of interest $\boldsymbol{\theta}$.

Lemma 2. *Suppose Assumptions (A1) holds. For any $\boldsymbol{\theta}, \tilde{\boldsymbol{\theta}} \in \Theta_\theta$, there exists a finite positive constant c_{12} , such that $\|\boldsymbol{\beta}(\boldsymbol{\theta}) - \boldsymbol{\beta}(\tilde{\boldsymbol{\theta}})\|_2 \leq c_{12}(m + p + K)\|\boldsymbol{\theta} - \tilde{\boldsymbol{\theta}}\|_2$.*

The third lemma is a Bernstein concentration inequality for the martingale $\int_0^T \{\lambda_i^y(t)dt - dY_i(t)\}$.

Lemma 3. *Suppose $a(t)$ is a non-negative \mathcal{H}_t -predictable process, and there is a finite positive constant c_{13} , such that $\sup_{t>0} a(t) \leq c_{13}$. Denote $M_i = \int_0^T a(t)\{\lambda_i^y(t)dt - dY_i(t)\}$, and $q_i = \int_0^T a^2(t)\lambda_i^y(t)dt$, $i = 1, \dots, m$. Then, for any $x > 0$, there exist some finite positive constants c_{14}, c_{15} , such that*

$$\Pr \left(M_i \geq \sqrt{2q_i x} + c_{15}x/3 \right) \leq \exp(-c_{16}x).$$

Lemma 3 provides the large deviation behavior of M_i , which is characterized by q_i , the bracket of the martingale. For the univariate case, if $a(t) = \dot{\lambda}_i(t)/\lambda_i(t)$, then q_i is equivalent to the variance of the score for an individual point process, and thus turns to be the Fisher information, which increases as the T increases. A similar observation holds for a multivariate point process.

5.2 Convergence properties

Next, we derive the asymptotic property for the penalized maximum likelihood estimator (MLE) of (20) with diverging dimensions of both the response and predictor processes. Since the parameter space grows along with the point process dimensions, we adopt the large-deviation approach

of Shen and Wong (1994); Shen (1998) to derive the asymptotics. Specifically, we consider a restricted parameter space for $\boldsymbol{\theta}$,

$$\Theta_{\boldsymbol{\theta}} = \left\{ \boldsymbol{\theta} : \|\boldsymbol{\theta}\|_{\infty} \leq c_0, p(\boldsymbol{\theta}) \leq c'_0{}^2 \right\},$$

where c'_0 is allowed to increase at the rate of $c'_0 = O(\sqrt{|\boldsymbol{\theta}|})$, and $|\boldsymbol{\theta}| = (m + p + K)R + m$ is the size of $\boldsymbol{\theta}$. Similarly, $|\boldsymbol{\beta}| = mpK + m$ and $|\mathcal{B}| = mpK$ denote the size of $\boldsymbol{\beta}$ and \mathcal{B} , respectively. We define a metric based on the Kullback-Leibler (KL) pseudo-distance for $\boldsymbol{\theta}, \tilde{\boldsymbol{\theta}} \in \Theta_{\boldsymbol{\theta}}$ as

$$d(\boldsymbol{\theta}, \tilde{\boldsymbol{\theta}}) = \mathbb{E} \left[\mathcal{L}\{\boldsymbol{\beta}(\boldsymbol{\theta})\} - \mathcal{L}\{\boldsymbol{\beta}(\tilde{\boldsymbol{\theta}})\} \right].$$

By Assumption (A5) and Ogata et al. (1978, Lemma 3), it is straightforward to verify that $d(\boldsymbol{\theta}, \boldsymbol{\theta}^0)$ is an appropriate distance metric for any $\boldsymbol{\theta} \in \Theta_{\boldsymbol{\theta}}$ with respect to the true value $\boldsymbol{\theta}^0$. Let $\hat{\boldsymbol{\theta}}$ denote the penalized maximum likelihood estimator of (20). The next theorem shows that $\hat{\boldsymbol{\theta}}$ converges to $\boldsymbol{\theta}^0$ exponentially in probability under the KL distance.

Theorem 1. *Suppose Assumptions (A1)-(A8) hold. For some $\varepsilon_1 > 0$, there exist finite positive constants c_{16}, c_{17} , such that*

$$\Pr \left\{ d(\boldsymbol{\theta}, \tilde{\boldsymbol{\theta}}) \geq \varepsilon_1 \right\} \leq 7 \exp \left\{ -c_{16} \frac{\pi_{\min}(\mathbf{J})}{\pi_{\max}(\mathbf{J})} T \eta_{|\mathcal{B}|}^2 \varepsilon_1^2 \right\},$$

where

$$\eta_{|\mathcal{B}|} = \frac{|\mathcal{B}|^{1/2}}{|\boldsymbol{\theta}|^{1/2}} \left[\log \left\{ \frac{|\mathcal{B}|(m + p + K)\sqrt{1 + c_{10}pK}}{c_{17}\sqrt{|\boldsymbol{\theta}|}} \right\} \right]^{-1/2},$$

and the penalty parameter τ in (20) satisfies that $\tau \leq O(T^{-1}\eta_{|\mathcal{B}|}^{-2})$.

Theorem 1 suggests that, the penalized MLE achieves a convergence rate of $\eta_{|\mathcal{B}|}\sqrt{T}$, which increases as T and $|\mathcal{B}|$ increase. The convergence rate of \sqrt{T} is due to the accumulated information from increasing number of observations, which is analogous to the sample size in a conventional regression model. On the other hand, in a traditional high-dimensional setting, the divergent dimension of the parameter space usually slows down the convergence rate of the model estimator (Chen et al., 2019b). This is not the case in our setting, where increasing dimensions of both the response and predictor processes also lead to a faster convergence rate. This is mainly because, with the low-rank structure (7), our model substantially reduces the size of the parameter space for the transferring coefficients. This enables us to obtain a smaller metric entropy with bracketing on

the parameter space, which in turn yields a better bound for the loss function and a faster convergence rate. We also briefly remark that, Theorem 1 holds for a general class of penalty functions, including both the sparsity penalty (8) and the subgrouping penalty (9), as long as Assumption (A8) is satisfied.

The convergence result in Theorem 1 is established under the KL distance, which is stronger than and usually dominates some other distance measures, e.g., the Hellinger metric. The next corollary provides the convergence of the recovered transferring coefficient under the L_2 -norm.

Corollary 1. *Suppose Assumptions (A1)-(A8) hold. Let $\hat{\mathbf{B}} = \mathbf{B}(\hat{\boldsymbol{\theta}})$ denote the recovered transferring coefficient tensor, and $\mathbf{B}^0 = \mathbf{B}(\boldsymbol{\theta}^0)$. For some $\varepsilon_2 > 0$, there exists a finite positive constant c_{18} , such that*

$$Pr \left(\frac{1}{|\mathbf{B}|^{1/2}} \|\hat{\mathbf{B}} - \mathbf{B}^0\|_F \geq \varepsilon_2 \right) \leq 7 \exp \left\{ -c_{18} \frac{\pi_{\min}(\mathbf{J})}{\pi_{\max}(\mathbf{J})} T \frac{|\mathbf{B}|}{|\boldsymbol{\theta}|} \varepsilon_2^2 \right\}.$$

Finally, we provide the theoretical result regarding the subgroup structure identification. Let $\mathcal{I}_1, \dots, \mathcal{I}_N$ denote a partition of the index set $\{1, \dots, m\}$, such that, for any $i \in \mathcal{I}_s$, $1 \leq s \leq N$, there is $\mathbf{B}^y[i, \cdot] = \boldsymbol{\beta}_{(s)}$. By definition, $\{\mathcal{I}_s\}_{s=1}^N$ refers to a subgroup structure that is allowed to grow as the number of response processes increases. In addition to the above regularity conditions, we need two more conditions. In particular, Assumption (A9) is placed to ensure the identifiability of the subgroups, which allows the number of subgroups to increase as the dimension of the response process increases. Assumption A(10) requires a local absolute continuity between $\boldsymbol{\beta}$ and $\boldsymbol{\theta}$, which holds as long as $\|\mathbf{B}\|_F$ is lower bounded away from zero.

(A9) There exists a finite positive constant c_{19} , such that $\min_{s \neq s'} \|\boldsymbol{\beta}_{(s)} - \boldsymbol{\beta}_{(s')}\|_2 > c_{19}$.

(A10) There exists a finite positive constant c_{20} , such that, for any $\boldsymbol{\beta}(\boldsymbol{\theta}), \boldsymbol{\beta}(\tilde{\boldsymbol{\theta}})$ in a neighborhood of $\boldsymbol{\beta}(\boldsymbol{\theta}^0)$, $\boldsymbol{\theta}, \tilde{\boldsymbol{\theta}} \in \Theta_{\boldsymbol{\theta}}$, we have $|\boldsymbol{\theta}|^{-1/2} \|\boldsymbol{\theta} - \tilde{\boldsymbol{\theta}}\|_2 \leq c_{20} |\boldsymbol{\beta}|^{-1/2} \|\boldsymbol{\beta}(\boldsymbol{\theta}) - \boldsymbol{\beta}(\tilde{\boldsymbol{\theta}})\|_2$.

Theorem 2. *Suppose Assumptions (A1)-(A10) hold. Let $(\mathbf{B}^y)^0$ and $\hat{\mathbf{B}}^y$ denote the true value and the estimator of the latent factor \mathbf{B}^y based on the objective function in (11). Suppose $\tau_s = o \left\{ \left(\frac{|\boldsymbol{\theta}|}{T|\mathbf{B}|} \right)^{1/2} \right\}$ and $\tau_f = O \left\{ \left(\frac{|\boldsymbol{\theta}|}{T|\mathbf{B}|} \right)^{1/2-\alpha} \right\}$ for some $0 < \alpha < 1/2$. Then, we have*

$$Pr \left(\hat{\mathbf{B}}^y[i, \cdot] = \hat{\mathbf{B}}^y[i', \cdot] \mid i, i' \in \mathcal{I}_s, 1 \leq s \leq N \right) \rightarrow 1, \text{ as } T \rightarrow \infty.$$

Theorem 2 shows that, as $T \rightarrow \infty$, the true subgroup structure can be identified with the probability tending to one, and our estimator achieves the subgroup identification consistency.

6 Simulations

6.1 Model with low-rank and sparsity structures

We study the finite-sample performance of our proposed method under different predictor processes $\mathbf{X}(t)$, including Poisson and Hawkes processes, different intensity link functions ϕ , including linear and logistic links, different low-dimensional structures, and varying number of parameters m, p and T . We first consider a model with the low-rank and sparsity structures in this section. We then consider a model with an additional subgroup structure in the next section.

We generate the data following model (6). Specifically, we first generate the p -dimensional predictor point process $\mathbf{X}(t)$. We consider two predictor processes, a homogeneous Poisson process with the marginal intensity Λ_j^x , and a Hawkes process with the transferring function $\omega_{jj'}(t) = \alpha_{jj'} e^{-\beta t}$ and the initial intensity $\Lambda_j^{(0)}$, where $\alpha_{jj'}$ is generated from a uniform distribution on $[0.2, 0.3]$, $\beta = 0.7$, and $j, j' = 1, \dots, p$. We consider two intensity link functions ϕ , a linear link and a logit link. For the linear link, we set the marginal intensity $\Lambda_j^x = 0.5$ for the Poisson predictor process, and set the initial intensity $\Lambda_j^{(0)} = 0.3$ for the Hawkes predictor process, $j = 1, \dots, p$. For the logit link, we set $\Lambda_j^x = 0.2$ for the Poisson process, and set $\Lambda_j^{(0)} = 0.15$ for the Hawkes process, $j = 1, \dots, p$. This way, the Poisson and Hawkes predictor processes are generated with similar levels of overall intensities. Next, we employ a mixture of three basis functions, $g^{(1)}(t) = \exp(-5t)$, $g^{(2)}(t) = 0.2 \mathbf{1}(t \leq 0.1)$, and $g^{(3)}(t) = 0.05 \mathbf{1}(t \leq 1)$. The first basis function is an exponential decay kernel that is widely used in point process modeling. The other two basis functions are piecewise indicator functions, and they are used to capture some “short-term” effect and “long-term” effect, respectively, motivated by neuronal spike trains analysis. Next, we generate the transferring coefficient tensor \mathcal{B} with a rank-3 structure, $\mathcal{B} = \sum_{r=1}^3 \nu_r \mathbf{b}_r^y \circ \mathbf{b}_r^x \circ \mathbf{b}_r^c$. For the linear link, we set $\nu = (0.3, 0.2, 0.3)^\top$,

$$\begin{aligned} \mathbf{b}_1^y &= \left((\boldsymbol{\eta}_1^y)_{m/2}^\top, \mathbf{0}_{m/2}^\top \right)^\top, & \mathbf{b}_1^x &= \left((\boldsymbol{\eta}_1^x)_{p/3}^\top, \mathbf{0}_{3p/4}^\top \right)^\top, \\ \mathbf{b}_2^y &= \left(\mathbf{0}_{5m/12}^\top, (\boldsymbol{\eta}_2^y)_{m/3}^\top, \mathbf{0}_{m/4}^\top \right)^\top, & \mathbf{b}_2^x &= \left(\mathbf{0}_{p/6}^\top, (\boldsymbol{\eta}_2^x)_{p/3}^\top, \mathbf{0}_{p/2}^\top \right)^\top, \\ \mathbf{b}_3^y &= \left(\mathbf{0}_{3m/4}^\top, (\boldsymbol{\eta}_3^y)_{m/4}^\top \right)^\top, & \mathbf{b}_3^x &= \left(\mathbf{0}_{2p/3}^\top, (\boldsymbol{\eta}_3^x)_{p/4}^\top, \mathbf{0}_{p/12}^\top \right)^\top, \end{aligned}$$

and \mathbf{b}_r^c , $\boldsymbol{\eta}_r^y$ and $\boldsymbol{\eta}_r^x$, $r = 1, 2, 3$, are all generated from a normal distribution with mean one and covariance the identity matrix. Figure 1(a) shows a slice of one generated coefficient tensor \mathcal{B} . For the logit link, we set $\nu = (0.2, 0.1, 0.2)^\top$, and generate $\mathbf{b}_r^y, \mathbf{b}_r^x, \mathbf{b}_r^c$ in the same way as for

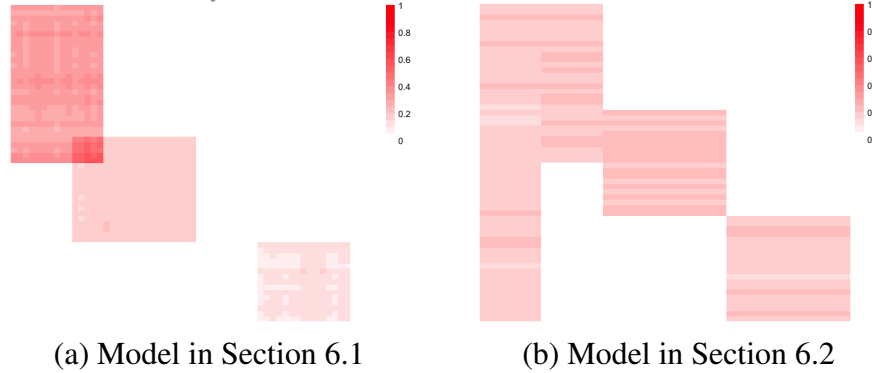


Figure 1: A slice of the true transferring coefficient tensor \mathcal{B} .

the linear link, except that we add a negative sign to each element of \mathcal{B} with probability 0.5. Finally, we set the background intensity $\mu = 0.01_m$, then generate the m -dimensional response point process $\mathbf{Y}(t)$ following model (6). Given the intensity function, each individual response process is simulated following the thinning strategy (Ogata, 1988). We set the dimensions of the response and predictor processes $m = p = \{60, 120\}$. We set the observed time interval length $T = \{800, 2000\}$. For a homogeneous point process, T plays the role of “sample size”, since it is proportional to the expected number of events. For an inhomogeneous point process, however, this is not necessarily true, and the expected number of observed events could vary across different marginal processes.

We compare our method with two alternative solutions. The first is to simply fit each of the response point process one at a time. The second is still to fit each response process one at a time, but adds a group L_1 penalty similarly as Hansen et al. (2015). We evaluate the estimation accuracy by the root mean square error (RMSE) of the estimated coefficient tensor \mathcal{B} .

Table 1 summarizes the results based on 50 data replications. It is seen that our proposed method consistently outperforms the two alternative solutions, as it achieves the smallest RMSE across all settings. As the time interval length T increases, all methods improve in estimation accuracy. On the other hand, as the numbers of point processes m and p increase, our method continues to improve, whereas the two alternative solutions suffer. This is largely due to that our method jointly model all the point processes together, instead of one at a time. Figure 2 shows the recovered transferring coefficient tensor \mathcal{B} for one data replication with a linear link and a Poisson predictor process. It is seen again that our method is capable of recovering the transferring structure successfully, while the other two methods cannot.

Table 1: Estimation accuracy of the transferring coefficient tensor \mathcal{B} for the model in Section 6.1. Three methods are compared: the one-at-a-time fitting method (Marginal), the one-at-a-time fitting method with a group L_1 penalty (Marginal- L_1), and our proposed method. Reported are the average RMSE based on 50 replications, with the standard errors in the parenthesis.

Link	Predictor	$m = p$	T	Marginal	Marginal- L_1	Our method
Linear	Poisson	60	800	0.281 (0.019)	0.234 (0.010)	0.147 (0.011)
			2000	0.168 (0.010)	0.149 (0.007)	0.094 (0.006)
	—	120	800	0.319 (0.025)	0.263 (0.021)	0.117 (0.015)
			2000	0.189 (0.011)	0.169 (0.009)	0.066 (0.009)
	Hawkes	60	800	0.307 (0.045)	0.279 (0.028)	0.185 (0.025)
			2000	0.226 (0.026)	0.197 (0.021)	0.125 (0.018)
—	120	800	0.337 (0.034)	0.289 (0.024)	0.129 (0.016)	
		2000	0.245 (0.015)	0.205 (0.010)	0.079 (0.010)	
Logit	Poisson	60	800	0.548 (0.026)	0.247 (0.015)	0.152 (0.012)
			2000	0.518 (0.015)	0.202 (0.009)	0.121 (0.009)
	—	120	800	0.844 (0.065)	0.264 (0.025)	0.134 (0.015)
			2000	0.645 (0.017)	0.196 (0.005)	0.101 (0.003)
	Hawkes	60	800	0.648 (0.045)	0.276 (0.028)	0.158 (0.025)
			2000	0.583 (0.035)	0.192 (0.018)	0.124 (0.012)
—	120	800	0.983 (0.048)	0.306 (0.026)	0.149 (0.014)	
		2000	0.725 (0.026)	0.211 (0.017)	0.103 (0.016)	

6.2 Model with additional subgrouping structure

We next consider a model with an additional subgrouping structure. For simplicity, we focus on the linear link ϕ and the Poisson predictor process. The results are similar for other combinations of link function and predictor process. We adopt the same simulation setup as in Section 6.1, except that we generate the transferring coefficient tensor \mathcal{B} in a different way. Specifically, we consider a rank-4 structure $\mathcal{B} = \sum_{r=1}^4 \nu_r \mathbf{b}_r^y \circ \mathbf{b}_r^x \circ \mathbf{b}_r^c$. We set $\nu = (0.2, 0.2, 0.2, 0.2)^\top$,

$$\begin{aligned}
 \mathbf{b}_1^y &= \left((\eta_1^y \mathbf{1})_{p/6}^\top, \mathbf{0}_{5p/6}^\top \right)^\top, & \mathbf{b}_1^x &= (\eta_1^x)_m, \\
 \mathbf{b}_2^y &= \left(\mathbf{0}_{p/6}^\top, (\eta_2^y \mathbf{1})_{p/6}^\top, \mathbf{0}_{2p/3}^\top \right)^\top, & \mathbf{b}_2^x &= \left((\eta_2^x)_{m/2}^\top, \mathbf{0}_{m/2}^\top \right)^\top, \\
 \mathbf{b}_3^y &= \left(\mathbf{0}_{p/3}^\top, (\eta_3^y \mathbf{1})_{p/3}^\top, \mathbf{0}_{p/3}^\top \right)^\top, & \mathbf{b}_3^x &= \left(\mathbf{0}_{m/3}^\top, (\eta_3^x)_{m/3}^\top, \mathbf{0}_{m/3}^\top \right)^\top, \\
 \mathbf{b}_4^y &= \left(\mathbf{0}_{2p/3}^\top, (\eta_4^y \mathbf{1})_{p/3}^\top \right)^\top, & \mathbf{b}_4^x &= \left(\mathbf{0}_{2m/3}^\top, (\eta_4^x)_{m/3}^\top \right)^\top,
 \end{aligned}$$

\mathbf{b}_r^c , η_r^x are all generated from a normal distribution with mean one and covariance the identity matrix, and η_r^y , $r = 1, 2, 3, 4$, are generated from a univariate normal distribution with mean one and variance 0.1. Note that, unlike the coefficient tensor in Section 6.1, here the entries are repeated in \mathbf{b}_r^y , which in turn induces the subgrouping structure. This structure can also be seen in Figure

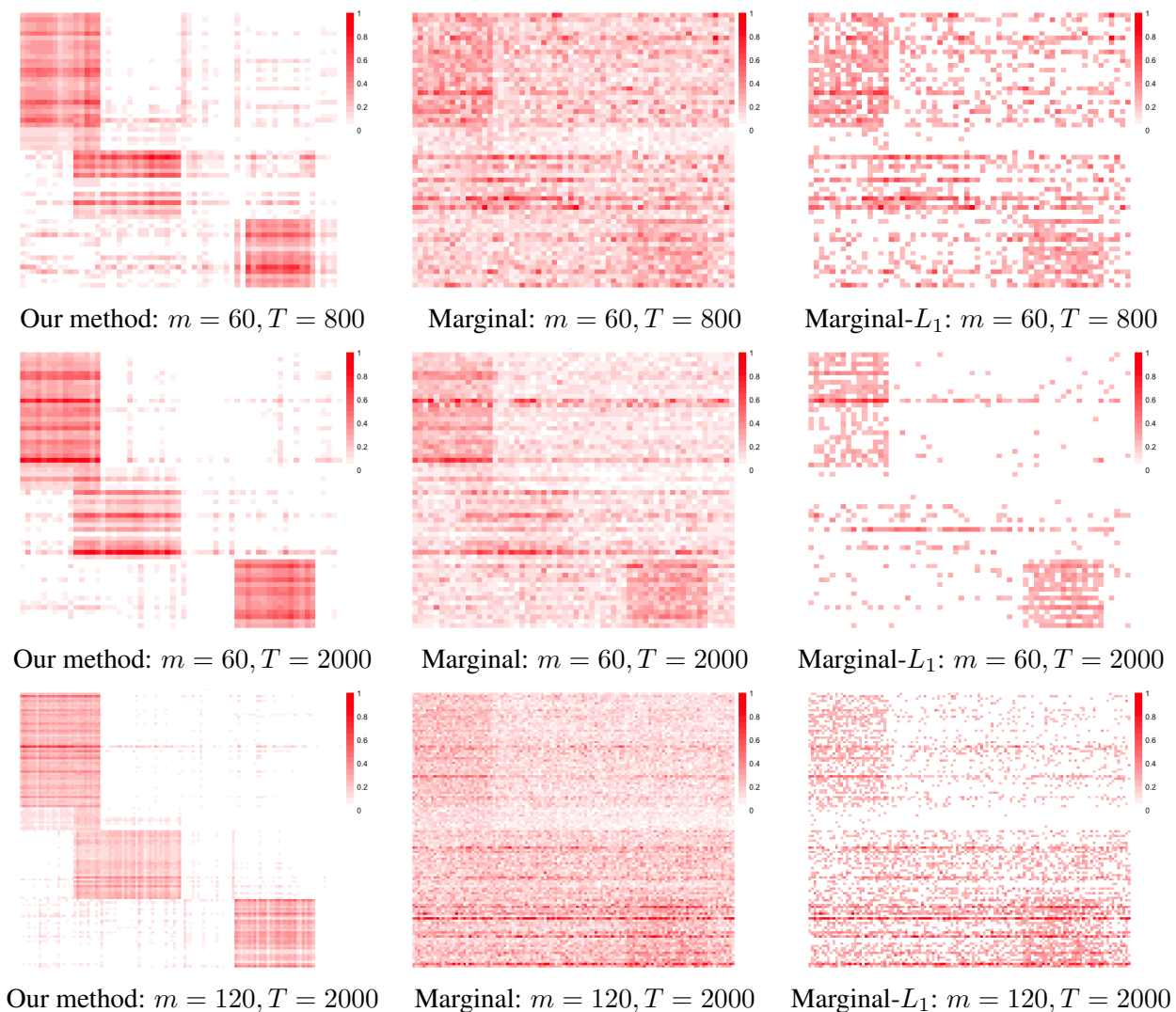


Figure 2: Recovered transferring coefficient tensor \mathcal{B} for the model in Section 6.1. Three methods are compared: the one-at-a-time fitting method (Marginal), the one-at-a-time fitting method with a group L_1 penalty (Marginal- L_1), and our proposed method.

1(b), which shows a slice of one generated coefficient tensor \mathcal{B} . We set the dimensions of the response and predictor processes $m = p = \{60, 120\}$, and the observed time interval length $T = \{1200, 2400\}$.

Table 2 summarizes RMSE based on 50 data replications, and Figure 3 shows the recovered transferring coefficient tensor \mathcal{B} for one data replication. It is again seen that our proposed method consistently outperforms the two alternative solutions in terms of estimation accuracy. Moreover, Table 2 includes the rand index statistic for our proposed method, which evaluates the clustering

Table 2: Estimation and clustering accuracy of the transferring coefficient tensor \mathcal{B} for the model in Section 6.2. Three methods are compared: the one-at-a-time fitting method (Marginal), the one-at-a-time fitting method with a group L_1 penalty (Marginal- L_1), and our proposed method. Reported are the average RMSE based on 50 replications, with the standard errors in the parenthesis. Rand index for our method is also reported.

$m = p$	T	Marginal	Marginal- L_1	Our method	{Rand Index}
60	1200	0.179 (0.026)	0.162 (0.013)	0.088 (0.010)	{0.854 (0.063)}
	2400	0.142 (0.012)	0.136 (0.008)	0.066 (0.005)	{0.909 (0.054)}
120	1200	0.219 (0.021)	0.179 (0.018)	0.073 (0.014)	{0.878 (0.099)}
	2400	0.169 (0.008)	0.147 (0.005)	0.052 (0.003)	{0.912 (0.071)}

performance. It is seen that our method achieves a high index value in all settings.

7 Cross-area Neuronal Spike Trains Analysis

Ensemble neural activity analysis is of central importance in system neuroscience, which aims to understand sensory coding and associations with motor output and cognitive functions (Brown et al., 2004; Kim et al., 2011). Some goals of common interest include the study of single-neuron activity with dependence on its own history, and the study of cross-neuron correlations based on spike trains similarities within the same area (Chen et al., 2019b). Beyond those goals, it is also of key interest to understand communication patterns in information transmission between neurons in different brain areas through neuronal spiking activities (Saalman et al., 2012). A group of neurons could be identified within a brain area based on their similar exciting or inhibitory effects onto another group of neurons in a different brain area. This hypothesis has been suggested by several scientific studies. For instance, (Liang et al., 2013) found that there might be discrete locations within the visual cortex area that respond to specific cross-modal inputs such as auditory or tactile. That is, the neurons in the V1 area are expected to be clustered in that they share similar cross-cortex-area association patterns (Liang et al., 2008), which needs to be inferred from the associations between the observed spike trains activities. In addition, the signal transmission takes time from one area to another, suggesting that the cross-area neuronal connection may account for a time-dependent convolutional effect rather than a simple co-firing. In recent years, benefitting from the rapid development of imaging techniques such as the calcium imaging, we are now able to monitor a large number of neurons simultaneously with a single-neuron resolution in a short time period, which produces high-dimensional point process type data of neuronal spike trains.

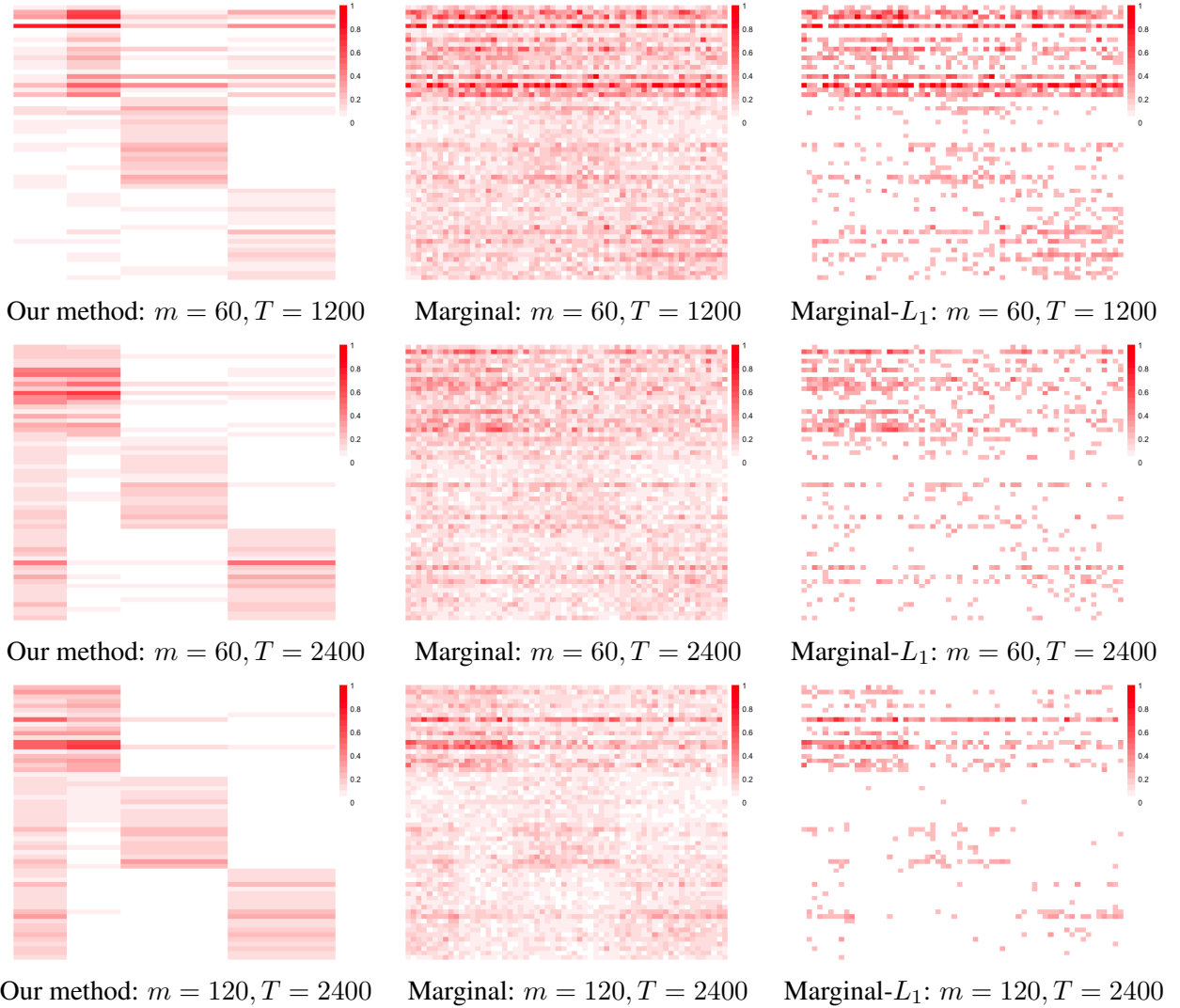


Figure 3: Recovered transferring coefficient tensor \mathcal{B} for the model in Section 6.2. Three methods are compared: the one-at-a-time fitting method (Marginal), the one-at-a-time fitting method with a group L_1 penalty (Marginal- L_1), and our proposed method.

In our study, we simultaneously measure the neuronal spike trains activities of 139 neurons and 283 neurons from two sensory cortical areas, A1 and V1, in a rat brain, respectively. We collect the data over 192 seconds under a stable stimulus. With 50 millisecond as a unit of time, we obtain the length of time interval of $[0, 3840]$. Figure 4 shows the recorded neuron firing events over time, and the histogram summary of the numbers of observed firings for individual neurons in each of these two areas. It is seen that most neurons have their numbers of observed firing events under 200, whereas a subset of neurons have the numbers below 100.

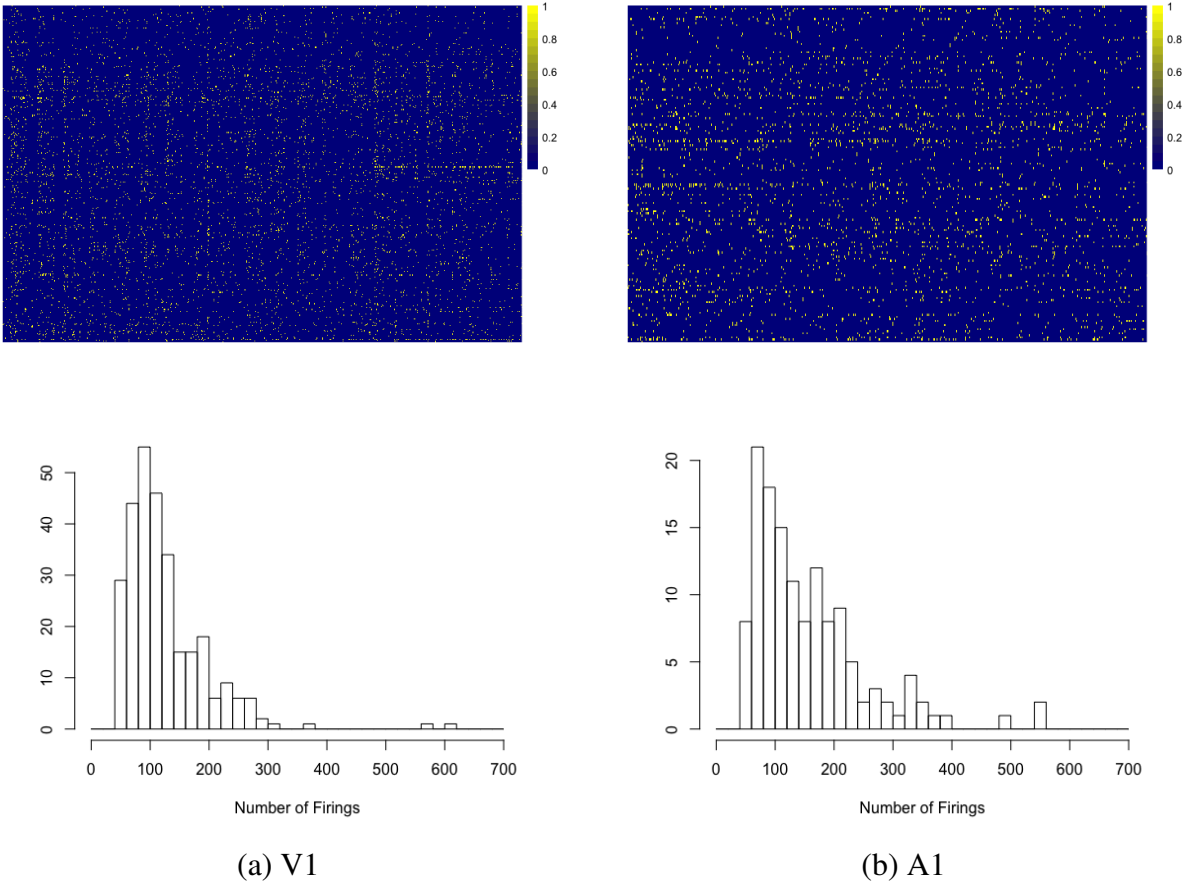


Figure 4: The neuron firings in the V1 and A1 areas. The heatmaps (upper panels) show the neuron-wise firings over time. The histograms (lower panels) summarize the number of firings for each neuron.

Our goal is to understand the information transmission from the A1 area to the V1 area. We fit the data using our proposed multivariate temporal point process regression, treating the neuronal spike trains in V1 as the response point process, and the neuronal spike trains in A1 as the predictor process. Since the observed firing events are sparse, we choose a logit link function. We select three basis functions, similarly as in our simulation studies: $g^{(1)}(t) = \exp(-t)$, $g^{(2)}(t) = 0.2 \mathbf{1}(t \leq 1)$, and $g^{(3)}(t) = 0.05 \mathbf{1}\{t \leq 5\}$, with the time intervals in the indicator functions selected based on the existing scientific findings that the communication process between ensemble neurons across areas mostly happens within tens of milliseconds (Luo et al., 2016). In addition to our proposed model, we also fit the marginal model that takes one response process at a time. Since some neurons have very limited number of firing events, the corresponding model fittings may not converge. Actually, for our data, we have found that about one third of the individual response process fittings cannot

Table 3: Evaluation of the model fitting for the cross-area neuronal spike trains analysis. Three methods are compared: the one-at-a-time fitting method (Marginal), the one-at-a-time fitting method with a group L_1 penalty (Marginal- L_1), and our proposed method.

	Marginal	Marginal- L_1	Our method
Deviance	0.388	0.256	0.185
AUC	0.537	0.579	0.682

converge. To handle this convergence issue, we add an L_2 regularization to this marginal approach, though we still refer to it as a marginal method. Moreover, we fit the marginal model with a group L_1 regularization, similarly as in our simulations.

To evaluate the model, we adopt a similar idea as Chen et al. (2019b), and split the point processes into a training set, i.e., the spike trains data in the time interval $[0, 2000)$, and a testing set, i.e., the data in the time interval $(2000, 3800]$. We report two evaluation criteria. The first criterion is the area under the ROC curve (AUC) based on a binary prediction (Luo et al., 2016). That is, we bin the continuous point process into a sequence of binary values based on a unit of time of 50 milliseconds, with one meaning that there is a firing event in this time bin, and zero otherwise. We then produce a sequence of binary predictions based on the predicted intensity function for the testing data. The second criterion is the deviance $\|\hat{\mathcal{B}}_{training} - \hat{\mathcal{B}}_{testing}\|$. That is, we obtain the estimated coefficient tensor \mathcal{B} from the training data and testing data, respectively, and evaluate the difference between the two in the Frobenius norm. Intuitively, if the firing patterns have been consistent, then this deviance measure should be small. Table 3 reports the results. It is seen that our proposed method achieves the highest AUC value and the lowest deviance value, suggesting a competitive performance of the proposed method compared to the two alternative solutions. We also identify five subgroups of neurons with our method, which requires future scientific validation, as we do not have relevant subgroup information for this dataset.

References

- Bacry, E., Gaïffas, S., and Muzy, J.-F. (2015). A generalization error bound for sparse and low-rank multivariate hawkes processes. *arXiv preprint arXiv:1501.00725*.
- Bacry, E. and Muzy, J.-F. (2016). First-and second-order statistics characterization of hawkes processes and non-parametric estimation. *IEEE Transactions on Information Theory*, 62(4):2184–2202.

- Boyd, S., Parikh, N., Chu, E., Peleato, B., Eckstein, J., et al. (2011). Distributed optimization and statistical learning via the alternating direction method of multipliers. *Foundations and Trends® in Machine learning*, 3(1):1–122.
- Brown, E. N., Kass, R. E., and Mitra, P. P. (2004). Multiple neural spike train data analysis: state-of-the-art and future challenges. *Nature neuroscience*, 7(5):456.
- Chen, B., He, S., Li, Z., and Zhang, S. (2012). Maximum block improvement and polynomial optimization. *SIAM Journal on Optimization*, 22(1):87–107.
- Chen, H., Raskutti, G., and Yuan, M. (2019a). Non-convex projected gradient descent for generalized low-rank tensor regression. *Journal of Machine Learning Research*, 20(5):1–37.
- Chen, S., Shojaie, A., Shea-Brown, E., and Witten, D. (2019b). The multivariate Hawkes process in high dimensions: Beyond mutual excitation. *arXiv preprint arXiv:1707.04928*.
- Cunningham, J. P., Byron, M. Y., Shenoy, K. V., and Sahani, M. (2008). Inferring neural firing rates from spike trains using gaussian processes. In *Advances in neural information processing systems*, pages 329–336.
- Daley, D. J. and Vere-Jones, D. (2007). *An introduction to the theory of point processes: volume II: general theory and structure*. Springer Science & Business Media.
- Diggle, P. J. (2013). *Statistical analysis of spatial and spatio-temporal point patterns*. Chapman and Hall/CRC.
- Diggle, P. J., Guan, Y., Hart, A. C., Paize, F., and Stanton, M. (2010). Estimating individual-level risk in spatial epidemiology using spatially aggregated information on the population at risk. *Journal of the American Statistical Association*, 105(492):1394–1402.
- Guan, Y. (2008). On consistent nonparametric intensity estimation for inhomogeneous spatial point processes. *Journal of the American Statistical Association*, 103(483):1238–1247.
- Guan, Y. (2011). Second-order analysis of semiparametric recurrent event processes. *Biometrics*, 67(3):730–739.
- Guan, Y., Jalilian, A., and Waagepetersen, R. (2015). Quasi-likelihood for spatial point processes. *Journal of the Royal Statistical Society: Series B (Statistical Methodology)*, 77(3):677–697.
- Hansen, N. R., Reynaud-Bouret, P., Rivoirard, V., et al. (2015). Lasso and probabilistic inequalities for multivariate point processes. *Bernoulli*, 21(1):83–143.

- Hawkes, A. G. (1971). Spectra of some self-exciting and mutually exciting point processes. *Biometrika*, 58(1):83–90.
- Ji, N., Freeman, J., and Smith, S. L. (2016). Technologies for imaging neural activity in large volumes. *Nature neuroscience*, 19(9):1154.
- Kang, J., Johnson, T. D., Nichols, T. E., and Wager, T. D. (2011). Meta analysis of functional neuroimaging data via bayesian spatial point processes. *Journal of the American Statistical Association*, 106(493):124–134.
- Kang, J., Nichols, T., Wager, T., and Johnson, T. (2014). A bayesian hierarchical spatial point process model for multi-type neuroimaging meta-analysis. *The Annals of Applied Statistics*, 8:1800–1824.
- Kim, S., Putrino, D., Ghosh, S., and Brown, E. N. (2011). A granger causality measure for point process models of ensemble neural spiking activity. *PLoS computational biology*, 7(3):e1001110.
- Kolda, T. G. and Bader, B. W. (2009). Tensor decompositions and applications. *SIAM review*, 51(3):455–500.
- Liang, M., Mouraux, A., Hu, L., and Iannetti, G. (2013). Primary sensory cortices contain distinguishable spatial patterns of activity for each sense. *Nature communications*, 4:1979.
- Liang, S., Carlin, B. P., and Gelfand, A. E. (2008). Analysis of minnesota colon and rectum cancer point patterns with spatial and nonspatial covariate information. *The annals of applied statistics*, 3(3):943.
- Luo, X., Gee, S., Sohal, V., and Small, D. (2016). A point-process response model for spike trains from single neurons in neural circuits under optogenetic stimulation. *Statistics in medicine*, 35(3):455–474.
- Ogata, Y. (1988). Statistical models for earthquake occurrences and residual analysis for point processes. *Journal of the American Statistical association*, 83(401):9–27.
- Ogata, Y. et al. (1978). The asymptotic behaviour of maximum likelihood estimators for stationary point processes. *Annals of the Institute of Statistical Mathematics*, 30(1):243–261.

- Okun, M., Steinmetz, N. A., Cossell, L., Iacaruso, M. F., Ko, H., Barthó, P., Moore, T., Hofer, S. B., Mrsic-Flogel, T. D., Carandini, M., et al. (2015). Diverse coupling of neurons to populations in sensory cortex. *Nature*, 521(7553):511.
- Perry, P. O. and Wolfe, P. J. (2013). Point process modelling for directed interaction networks. *Journal of the Royal Statistical Society: Series B (Statistical Methodology)*, 75(5):821–849.
- Pillow, J. W., Shlens, J., Paninski, L., Sher, A., Litke, A. M., Chichilnisky, E., and Simoncelli, E. P. (2008). Spatio-temporal correlations and visual signalling in a complete neuronal population. *Nature*, 454(7207):995.
- Rathbun, S. L. and Cressie, N. (1994). Asymptotic properties of estimators for the parameters of spatial inhomogeneous poisson point processes. *Advances in Applied Probability*, 26(1):122–154.
- Saalmann, Y. B., Pinsk, M. A., Wang, L., Li, X., and Kastner, S. (2012). The pulvinar regulates information transmission between cortical areas based on attention demands. *Science*, 337(6095):753–756.
- Shen, X. (1998). On the method of penalization. *Statistica Sinica*, 8(2):337–357.
- Shen, X. and Wong, W. H. (1994). Convergence rate of sieve estimates. *The Annals of Statistics*, pages 580–615.
- Sidiropoulos, N. D. and Bro, R. (2000). On the uniqueness of multilinear decomposition of n-way arrays. *Journal of Chemometrics*, 14(3):229–239.
- Stoyan, D., Penttinen, A., et al. (2000). Recent applications of point process methods in forestry statistics. *Statistical Science*, 15(1):61–78.
- Sun, W. and Li, L. (2017). Store: Sparse tensor response regression and neuroimaging analysis. *Journal of Machine Learning Research*, 18:4908–4944.
- Tang, X., Bi, X., and Qu, A. (2019). Individualized multilayer tensor learning with an application in imaging analysis. *Journal of the American Statistical Association*.
- Waagepetersen, R. and Guan, Y. (2009). Two-step estimation for inhomogeneous spatial point processes. *Journal of the Royal Statistical Society: Series B (Statistical Methodology)*, 71(3):685–702.

- Wang, Y., Xie, B., Du, N., and Song, L. (2016). Isotonic hawkes processes. In *International conference on machine learning*, pages 2226–2234.
- Wang, Y., Yin, W., and Zeng, J. (2019). Global convergence of admm in nonconvex nonsmooth optimization. *Journal of Scientific Computing*, 78(1):29–63.
- Yuan, M. and Lin, Y. (2006). Model selection and estimation in regression with grouped variables. *Journal of the Royal Statistical Society: Series B (Statistical Methodology)*, 68(1):49–67.
- Zhang, A. and Han, R. (2019). Optimal sparse singular value decomposition for high-dimensional high-order data. *Journal of the American Statistical Association*, 0(0):1–34.
- Zhang, C.-H. et al. (2010). Nearly unbiased variable selection under minimax concave penalty. *The Annals of statistics*, 38(2):894–942.
- Zhou, H., Li, L., and Zhu, H. (2013a). Tensor regression with applications in neuroimaging data analysis. *Journal of the American Statistical Association*, 108(502):540–552.
- Zhou, K., Zha, H., and Song, L. (2013b). Learning social infectivity in sparse low-rank networks using multi-dimensional hawkes processes. In *Artificial Intelligence and Statistics*, pages 641–649.
- Zhu, X., Tang, X., and Qu, A. (2019). Longitudinal clustering for heterogeneous binary data. *Statistica Sinica*.